Catena 203 (2021) 105368

Contents lists available at ScienceDirect

Catena

journal homepage: www.elsevier.com/locate/catena

Behavioral differences between weathering and pedogenesis in a subtropical humid granitic terrain: Implications for chemical weathering intensity evaluation

Haowei Mei, Xing Jian *, Wei Zhang, Hanjing Fu, Shuo Zhang

State Key Laboratory of Marine Environmental Science, College of Ocean and Earth Sciences, Xiamen University, Xiamen 361102, PR China

ARTICLE INFO

Keywords:
Regolith
Soil
Element mobility
Weathering index
Clay minerals

ABSTRACT

Continental weathering plays a crucial role in the evolution of the Earth's surface by linking Earth's spheres, shaping landscapes and regulating chemical cycles and global climate. Regolith weathering studies in some cases ideally assume successive and progressive bottom-up physicochemical variation trends. To validate this assumption, we target a granitic regolith profile in a subtropical monsoon climate-dominated region (southeast China). We present mineralogical, petrographic and geochemical data from soil, saprolite and bedrock samples to characterize physical and chemical alterations. The petrographic and mineralogical results indicate that both plagioclase and K-feldspar are depleted and kaolinite is the major neoformed mineral phase in top-soil samples, revealing intensive chemical weathering on the regolith. However, these top-soil samples have much lower chemical index of alteration (CIA, ca. 64–67) values than the underlying oxidized-soil samples (CIA values ranging 65–80). Some chemically immobile elements, such as Al, Ti, Zr and Hf, are depleted in top-soil samples but are comparatively enriched in oxidized-soil samples. This is attributed to vertical leaching and translocation of fine-grained minerals (e.g., kaolinite, illite and zircon) through the soils. Furthermore, the analyzed top-soil samples are comparatively rich in elements K and P, which are most likely due to the evident biological fixation process. These physical and biological processes in the unconsolidated, porous and biotic top-soil layer can be responsible for the unexpected low CIA values. Our findings demonstrate the complex physical, chemical and biological alterations on soils and the differential behaviors between weathering and pedogenic processes, especially for those tropical–subtropical high rainfall regions. This case study also highlights the importance of petrographic and mineralogical proxies to chemical weathering intensity evaluation for regolith profiles and siliciclastic sediments.

1. Introduction

When rocks meet with water, atmosphere and biota, they can be corroded and weathered into different forms, such as water-soluble ions, neoformed minerals and residual complexes. As a vital process controlling the Earth' surface evolution (Jin et al., 2010; Jian et al., 2019), weathering is a significant process to long-term climate regulation (Walker et al., 1981; Berner, 1995; Kump et al., 2000; Goddéris et al., 2008), soil formation (Heimsath et al., 1997; Rihs et al., 2016), global geochemical cycles (Hodell et al., 1990; West et al., 2005; Bouchez and Gaillardet, 2014) and life sustenance (Brantley et al., 2007; Brantley, 2008; Rajamani et al., 2009).

Previous studies on weathering have highlighted the importance of geochemical behaviors (e.g., Parker, 1970; Nesbitt et al., 1980; Nesbitt and Young, 1982; Middelburg et al., 1988; Price and Velbel, 2003) and petrographic or mineralogical transformations (e.g., Blum and Erel, 1997; Kretzschmar et al., 1997; Taboada and García, 1999; Le Pera et al., 2001; Braga et al., 2002; Campodonico et al., 2014) for understanding and quantifying weathering processes at the Earth's surface. And these studies have been conducted from a variety of perspectives, such as river catchments (e.g., Stallard and Edmond, 1983; White and Blum, 1995; Louvat and Alle'gre, 1997; Gaillardet et al., 1999; Stewart et al., 2001; Dessert et al., 2003; Oliva et al., 2003; Su et al., 2017), sediments (e.g., McLennan, 1993; Nesbitt and Markovics, 1997; Young and Nesbitt, 1998; Wallmann et al., 2008; Wei et al., 2006; Sharma et al., 2013; Fedo et al., 2015; Thorpe et al., 2019; Thorpe and Hurowitz, 2020) and in-situ

* Corresponding author.
E-mail address: xjian@xmu.edu.cn (X. Jian).

https://doi.org/10.1016/j.catena.2021.105368
Received 6 July 2020; Received in revised form 12 March 2021; Accepted 7 April 2021

regolith profiles (e.g., Condie et al., 1995; Young and Nesbitt,1998; Price and Velbel, 2003; Dosseto et al., 2008; Liu et al., 2016; Scarciglia et al., 2016; Li et al., 2021).

In-situ chemical weathering processes of regolith profiles are always coupled with pedogenesis. As in-situ physical and chemical weathering proceeds, downward movement of the weathering front promotes the development of soils. Both weathering and pedogenic processes involve transforming coherent rocks into loose mineral materials, which can be recombined to form silicate clays or other secondary minerals. In this manner, biochemical processes during weathering transform primary geologic materials into the compounds of which soils are made (Brady and Weil, 2008). As these two processes transfer elements from primary phases to secondary products and eliminate geochemical information about the parent materials (Nesbitt and Markovics, 1997), they can be deciphered through mineralogical, geochemical and textural features (e.g., clay minerals, elemental concentrations, isotopic signatures, porosity, grain size and morphology) (Brantley and Lebedeva, 2011).

Chemical weathering-related investigations sometimes ideally assume successive and progressive bottom-up variation (e.g., textural, mineralogical and geochemical) trends for a regolith profile, i.e., ignoring potential behavioral differences between pedogenic and weathering processes. The compositions of soil parent materials are similar to that of the upper part of a weathering profile (near the weathering front), which can be transformed into soils through years of climate-induced biological processes. Climatic factors, particularly precipitation and temperature, dramatically influence soil properties by affecting types and rates of physical, chemical, and biological processes (Dahlgren et al., 1997). Under warm and humid climatic conditions, pedogenesis prevails along with intensive alteration of primary minerals, neoformation of Fe and Al-oxides, rapid mineralization of organic carbon, and non-negligible leaching potential (Middelburg et al., 1988; Macias and Chesworth, 1992; Dahlgren et al., 1997; Wilson, 1999; Podwojewski et al., 2011).

Abundant precipitation, high humidity and flat surfaces promote the moisture storage capacity of soils and further enhance weathering (Phillips et al., 2008). Soil development and its thickness depends on an equilibrium between erosion and weathering (Rihs et al., 2016). In a tectonically active zone, weathering can barely keep up with the rate of erosion, resulting in mostly thin, weathering-limited soils (Yaalon, 1997). However, if the regolith profiles are under tectonically stable conditions, the soils are thick and therefore can be a significant target to study weathering and pedogenesis. Furthermore, there are complex interactions between soil biotic and abiotic components within a top-soil system (Zhu et al., 2014). All these factors can result in diverse regolith profiles and textural heterogeneity within a regolith profile. This might lead to differential physical and chemical behaviors during weathering and pedogenic processes (Kabata-Pendias and Pendias, 2001). In this case, caution should be exercised when investigating weathering dynamics, mechanisms and products based on in-situ regolith profiles.

In this study, we focus on a granitic regolith profile located in southeastern China with a wet subtropical climate. We present mineralogical, petrographic and geochemical data to discuss in-situ physical and chemical alterations of the regolith profile under such conditions and to have a better understanding of dynamics of weathering and pedogenic processes.

2. Regional background

The investigated granitic regolith profile is located in Xiamen, Fujian province, southeast China (24°38′8″ N, 118°18′27″ E). The landscape is characterized by hilly terrane (the elevation here is less than 180 m), and is covered with subtropical grassy vegetation and trees. Elevation of the profile is 79 m above sea level. The mean annual temperature is 21 °C and the mean annual precipitation is 1200–1400 mm, the East Asian summer monsoon generates about 60–85% of the annual total precipitation (Su et al., 2015). Due to typical monsoon climate and episodic typhoon events (Jian et al., 2020a, 2020b), rainfall in this region is distributed unevenly through the year, including an intense rainy period (from April to September) and relatively dry conditions in the rest of the year (Fig. 1C). The widespread granitoid rocks in this region were formed by the subduction of the Paleo-Pacific Plate beneath the Eurasian

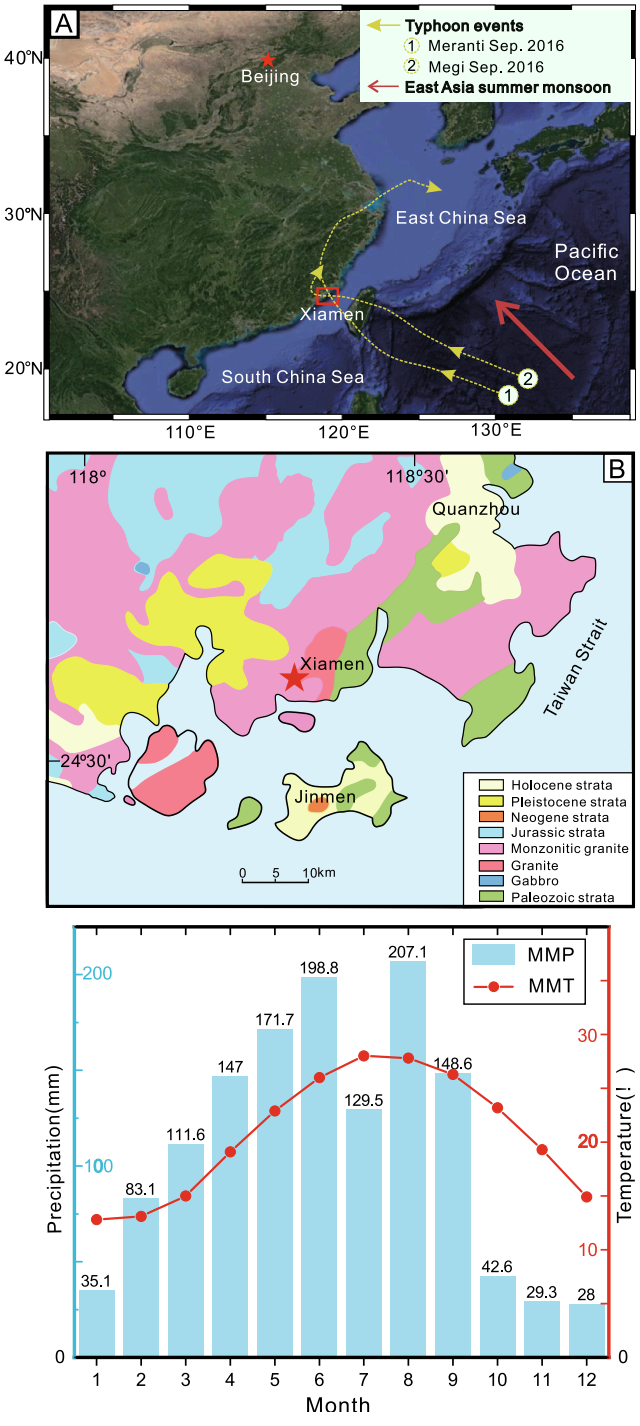

Fig. 1. (A) Location of the study area. The paths of representative typhoons were collected from the website http://typhoon.weather.com.cn. (B) Geologic map showing location of weathering profile in this study and associated bedrock units. (C) Average monthly temperature and precipitation in the study area. Data are from China meteorological administration and based on the average between 1981 and 2010. MMP: mean monthly precipitation. MMT: mean monthly temperature.

continent in the Late Mesozoic (Li et al., 2014), and currently were under a tectonically stable background.

3. Materials and methodology

3.1. Sample collection

The investigated samples include soils and alteration zones below the soil down to the bedrock. We refer to the definitions of layers used by Berger et al. (2014) and divided the whole profile into four layers with different alteration degrees from bottom to top: bedrock (3.3–4.4 m of depth, layer 1; firm, unaltered or slightly altered protolith); saprolite (1.5–3.3 m of depth, layer 2; weak, brittle, altered rock material with the texture and structure of the bedrock); oxidized-soil (0.6–1.5 m of depth, layer 3; dark-red and not showing layering or structure of bedrock, without plant roots); top-soil (0–0.6 m of depth, layer 4; dark-brown, soft and porous texture, abundant plant roots). Each sample was spaced 20 to 30 cm apart (Fig. 2) and a total of 22 samples were collected. All samples were taken from outcrops 10–15 cm within the external surface.

3.2. Analytical procedures

Samples selected from the fresh bedrock layer were directly made to 30 μm -thick standard thin sections, and samples from other layers were first impregnated with araldite and then cut into thin sections for traditional petrographic study (Jian et al., 2020a). These thin sections were observed under a polarizing microscope and were analyzed by counting more than 400 points using the Gazzi-Dickinson method (Dickinson, 1985). The point-counting spacing interval was constant for each thin section and was dependent on the sizes of major crystals in the analyzed samples. Each mineral was identified and counted according to whether it was weathered, and microfractures and voids were also counted.

Samples for bulk mineralogical and geochemical analysis were first crushed and then grinded to 200 mesh in an agate mortar. A Rigaku Ultima IV X-ray diffractometer (XRD) at Xiamen University was used for the analysis of bulk powder mineral and clay fraction (<2 μm) compositions. To obtain clay fractions, about 4 g sample (for the oxidized-soil and top-soil samples) was soaked in deionized water, then was dispersed by using an ultrasonic oscillator. Clay flocculation was avoided by adding 0.1 g of sodium hexametaphosphate. Saprolite and bedrock samples were first roughly crushed and were then treated following the same procedure. The particles <2 μm were separated according to the Stoke's law and were concentrated in a centrifuge. Thereafter, organic materials and carbonate were removed by hydrogen peroxide (10%) and acetic acid (15%), respectively (Wan et al., 2007, 2010). The wet concentrated particles were placed on glass slides, air-dried and made as oriented mounts. These oriented mounts were then placed in a vacuum pressure box and were saturated with ethylene glycol vapor for at least 48 h. Exposing the air-dried oriented mount to this condition can promote the exchange of ethylene glycol molecules into the interlayer spacing of swelling clays and thus produce a characteristic expansion in these phases (Moore and Reynolds, 1997; Thorpe et al., 2019). Each sample was constantly scanned under 40 kV, 30 mA, wave length of 1.54 and step width of 0.02° conditions. Scanning speeds were 4°/min for bulk powder and clay fraction analysis. A MDI jade software was used for data smoothing, peak value extraction and phase identification. Semi-quantitative determinations of bulk mineral mounts were conducted utilizing integrated peak areas and empirical reference intensity ratio (RIR) factors (Kamp, 2010). Relative percentages of smectite, illite, kaolinite and chlorite were determined using ratios of integrated peak areas of (001) series of their basal reflections according to the XRD diagrams of ethylene-glycol treated mounts, and were weighted by empirically estimated factors (Biscaye, 1965; Wan et al., 2010; He et al., 2013; Liu et al., 2017).

A X-ray fluorescence (XRF) spectrometer was employed for major elements determinations after removing organic materials. The sample powders were mixed with lithium metaborate flux at 1:10 and melted at 1050 °C in a Pt-Au crucible. The well-mixed melt was cooled and then a glass disk was used for XRF analysis. The loss on ignition (LOI) values were obtained by measuring the mass reduction after heating the sample at 980 °C. The detailed analytical procedures were after Liu et al. (2012).

Trace and rare earth elements analysis was performed by an ICP-MS. Before mass spectrum analysis, the sample powders were accurately weighed (25 mg) and placed in high-pressure-resistant Teflon beakers, with a 1:1 mixture of HF-HNO_3 and heated for 24 h at 80 °C, and then evaporated. When solutions were evaporated to nearly dry, 1.5 ml HNO_3, 1.5 ml HF and 0.5 ml $HClO_4$ were added respectively and the beakers with solutions were capped for digestion within a high-temperature oven at 180 °C for at least 48 h until the samples were completely dissolved. Then, the solutions were diluted with 1% HNO_3 to 50 ml for determination. Analytical precision and accuracy were monitored by international standards GSR-5 and GSD-11. The results show that most of the relative deviations between measured and certified values are generally less than 20%.

3.3. Weathering intensity quantification

Weathering indices are effective tools in characterizing weathering profiles and in quantitatively assessing weathering intensity. Many researchers have proposed various weathering indices on the basis of

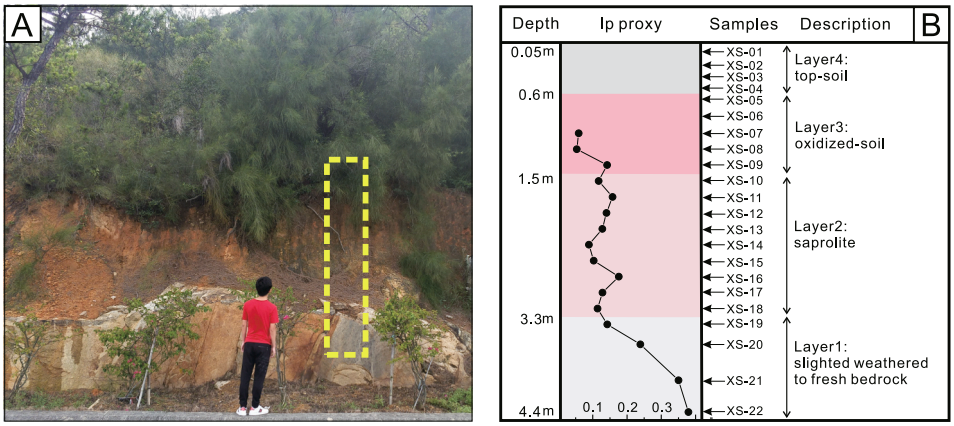

Fig. 2. (A) Outcrop photograph of the investigated regolith profile. (B) Sample position and layers in the profile. Ip proxy: Micropetrographic Index, devised by Irfan and Dearman (1978), see the related sentences in the main text for the detailed calculation. Relatively lower Ip values in upper layer samples indicate more intense weathering intensity.

mineralogical (Esquevin, 1969; Chamley, 1989; Clift et al., 2014), petrographic (Irfan and Dearman, 1978; Nesbitt and Young, 1996; Kamp, 2010; Andò et al., 2012) and geochemical (Parker, 1970; Nesbitt and Young, 1982; Harnois, 1988; Fedo et al., 1995; Price and Velbel, 2003 and references therein) data. Here, the commonly used indices, Micropetrographic Index, kaolinite/illite, quartz/(quartz + feldspar), illite chemistry index, Chemical Index of Alteration, Chemical Index of Weathering and Plagioclase Index of Alteration are selected to discuss weathering intensity for this profile. The Micropetrographic Index (Ip) (Fig. 2), devised by Irfan and Dearman (1978), is defined as a ratio among unweathered primary minerals and weathered components (including secondary phases together with microcracks and voids). Kaolinite/illite (Chamley, 1989; Clift et al., 2014) is based on the clay fraction XRD patterns and quartz/(quartz + feldspar) (Kamp, 2010) is based on the bulk mineralogical XRD analysis data. Illite chemistry index refers to the ratio of the 5 Å and 10 Å peak areas (Esquevin, 1969). The Chemical Index of alteration (CIA), proposed by Nesbitt and Young (1982), is calculated as the ratio [$Al_2O_3/(Al_2O_3 + CaO^* + Na_2O + K_2O)$ *100] in molecular proportions, where CaO* represents the amount of CaO incorporated in the silicate fraction only. The proxy CIA assumes that Al_2O_3, Na_2O, K_2O and CaO reside exclusively in feldspar and Al_2O_3 is conserved during weathering. Harnois (1988) proposed a modified index, Chemical Index of Weathering (CIW), which is calculated as the ratio [$Al_2O_3/(Al_2O_3 + CaO + Na_2O)$ * 100]. Potassium therein was eliminated from the proxy calculation because K has more complicated geochemical behavior during weathering than Ca and Na. Fedo et al. (1995) further introduced a new index, Plagioclase Index of Alteration (PIA), calculated as [$(Al_2O_3\text{-}K_2O)/(Al_2O_3 + CaO + Na_2O\text{-}K_2O)$ * 100] to characterize chemical weathering degrees of plagioclase. Details of these chemical indices have been well summarized in Price and Velbel (2003).

4. Results

4.1. Petrography

Bedrock thin section observation results (Table 1) indicate that the parent materials of the regolith profile are monzonitic granite. Fresh samples primarily consist of plagioclase (55%), quartz (35%), K-feldspar (7%) and accessory minerals mainly including biotite, muscovite and hornblende. Saprolite samples are characterized by abundant microfractures and voids (Fig. 3D-E) and slight plagioclase sericitization (Fig. 3C). The oxidized-soil samples have been strongly eroded (Fig. 3A-B), minerals in these samples show more significant alterations compared to saprolite samples. The crack systems are characterized by inter-, intra-, and transgranular microcracks. Progressive weathering produces a dusty appearance with alteration advancing along cleavages and fractures on minerals in these samples, and features of some minerals are erased and barely discernible. Quartz remains abundant and pervasive but its grains decrease in size because of fractures. Point counting-based modal compositions of the analyzed samples are shown in Table 1. For the oxidized-soil and saprolite samples, plagioclase abundances are low but K-feldspar and fracture proportions are relatively high, compared to the fresh bedrock samples. (Fig. 3).

4.2. Mineral compositions based on XRD analysis

Representative bulk and clay fraction (i.e., <2 μm) XRD patterns of the analyzed samples are shown in Fig. 4. XRD patterns of the bulk samples indicate that the fresh bedrock samples principally consist of quartz, K-feldspar and plagioclase. It is consistent with the petrographic results mentioned above. By contrast, upper weathered samples (e.g., Samples XS-02 and XS-07) indicate K-feldspar peaks are weak and plagioclase peaks have disappeared (Fig. 4A). XRD patterns of the clay fractions reveal that kaolinite and illite are two major clay minerals in the upper profile (Fig. 4B).

4.3. Major element compositions

Major element geochemical data are illustrated with depths in Fig. 5A and are presented in Table A1 (in the Supplementary Material). The layers 1–2 have lower SiO_2 (72.9–77.8 wt%) and Fe_2O_3 (T) (0.49–1.70 wt%) contents compared with the top-soil and oxidized-soil layers. The layers 3–4 show significant depletion in Al_2O_3 (8.82–14.66 wt%), CaO (<0.07 wt%), Na_2O (0.25–0.37 wt%) and K_2O (3.36–4.20 wt %). Samples from the oxidized-soil layer indicate relatively obvious high LOI (up to 4.57% wt%) and Fe_2O_3 (T) (up to 3.03% wt%) values. It is worth noting that the LOI values show similar vertical variation trends to that of Al_2O_3 contents, both of which reach peak values at the bottom of oxidized-soil layer.

4.4. Trace-and rare earth element compositions

Trace- and rare earth elemental data are shown in Table A1. Fig. 5B displays the variations of representative trace- and rare earth element (REE) contents with sampling depths. The results reveal that the upper

Table 1
Petrographic modal compositions and micropetrographic index (Ip).

Sample	Modal compositions based on point-counting data					Micropetrographic index calculation		
	Qtz	Pl	Kfs	Others	Microfractures and voids	Unweathered	Weathered	Ip
XS-07	38.6	35.6	16.4	1.3	8.1	5.6	86.4	0.06
XS-08	28.7	20.2	13.9	28.4	8.8	5.0	86.1	0.05
XS-09	34.7	33.8	20.7	4.1	6.7	12.4	80.9	0.14
XS-10	40.3	29.2	19.7	3.2	7.6	10.5	81.9	0.12
XS-11	43.0	30.7	15.5	4.1	6.6	13.6	79.7	0.16
XS-12	42.5	33.3	15.1	2.2	6.9	12.3	80.8	0.14
XS-13	40.1	38.5	13.6	3.5	4.3	11.3	84.4	0.13
XS-14	39.7	47.3	7.6	2.8	2.5	8.1	89.3	0.09
XS-15	40.8	44.3	10.3	1.3	3.3	9.3	87.4	0.10
XS-16	38.5	50.2	5.6	0.0	5.6	15.0	79.4	0.18
XS-17	40.2	46.0	7.6	3.3	3.0	11.4	85.6	0.13
XS-18	40.3	46.0	6.5	4.0	3.2	10.2	86.6	0.11
XS-19	40.9	47.4	6.5	3.0	2.2	12.5	85.3	0.14
XS-20	37.0	46.5	12.1	1.5	2.8	19.3	77.9	0.24
XS-21	36.8	52.6	6.3	1.0	3.3	25.9	70.8	0.35
XS-22	35.8	55.0	7.1	0.4	1.7	27.5	70.8	0.38

The modal data are in volume percent. The micropetrographic index (Ip) was proposed by Irfan and Dearman (1978). Qtz: quartz, Pl: plagioclase, Kfs: K-feldspar, Unweathered: unweathered primary minerals, Weathered: weathered minerals including neoformed phases, Ip = unweathered/(weathered + microfractures and voids). Others mainly include accessory minerals (e.g., biotite, hornblende, muscovite) and neoformed minerals.

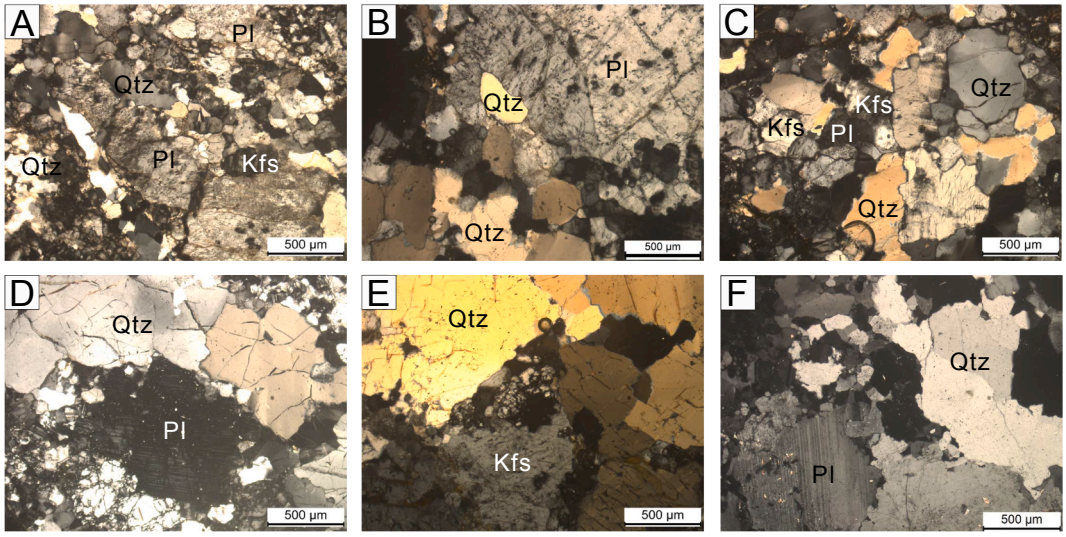

Fig. 3. Representative photomicrographs of the analyzed samples. (A) and (B) the plagioclase grain was significantly altered and the outlines of the minerals are vague (Sample XS-07 and Sample XS-09, respectively); (C) plagioclase has undergone moderate weathering (Sample XS-11); (D) and (E) are characterized by intensive microfractures within quartz grains (Sample XS-16 and XS-17, respectively); (F) slightly weathered plagioclase and quartz from bedrock (Sample XS-21). Qtz: quartz, pl: plagioclase, Kfs: K-feldspar. All the photomicrographs were taken under the cross-polarized light.

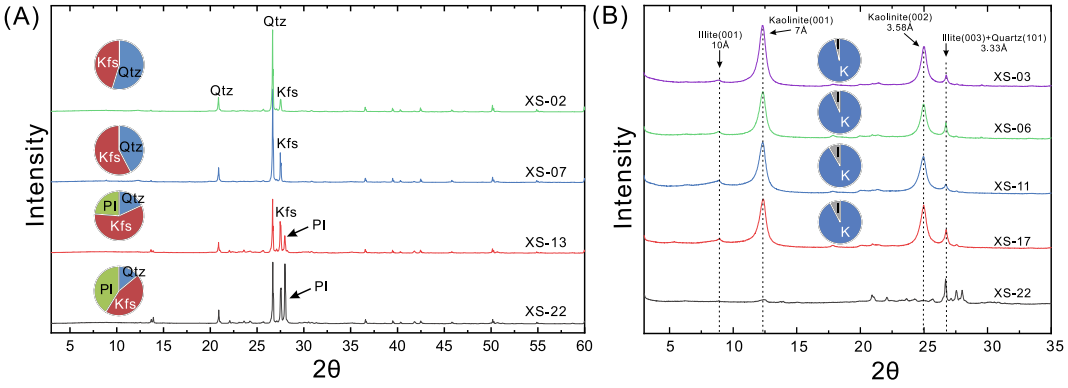

Fig. 4. (A) Bulk XRD analysis results of selected samples. Pie charts indicate relative abundances of quartz, K-feldspar and plagioclase based on XRD pattern interpretations. Note that characteristic peaks of plagioclase haven't been found in samples XS-02 and XS-07. (B) Clay fraction (i.e., <2 μm) XRD patterns of selected samples. Pie charts indicate relative abundances of kaolinite and illite. Illite is an immature weathering product and can transform into kaolinite during extreme weathering in top-soil layer sample (XS-03). Qtz: quartz, Pl: plagioclase, Kfs: K-feldspar, K: kaolinite, I: illite.

two layers showing remarkable depletion in Be and Yb, slight depletion in Ba, Sr and Th. Zr and Hf co-varied in the profile and were enriched in soils. The contents of Sc and La do not have correlations with depths. Fig. 6 displays Chondrite-normalized REE patterns of all the samples along the profile. It is notable that the samples in saprolite show positive Ce anomalies (chondrite-normalized, with the Ce/Ce* ranges from 1.32 to 4.57) compared with other samples (Fig. 6, Table A1), which may cause ∑LREE to reach its maximum value in this layer (Fig. 5).

4.5. Weathering intensity

The results of weathering indices are shown in Fig. 7. The mineralogical weathering indices (Fig. 7) have comparatively higher values in soils samples. Both Kaolinite/illite and illite chemistry index reach their maximum values at the top-soil. The quartz/(quartz + feldspar) ratio values in top-soil and oxidized-soil layers are obviously higher than that in the lower part of the profile. The CIA, CIW and PIA values are ranging in 50.1–77.8, 64.4–96.5 and 51.1–95.3, respectively, increase from bedrock to oxidized-soil samples but tend to decrease from oxidized-soil to top-soil samples (remarkably for CIA values and slightly for CIW and PIA values, Fig. 7).

5. Discussion

5.1. Physical and chemical weathering intensity evaluation of the profile

Physical alteration was evaluated through thin section petrographic results. The analyzed samples show increasing physical fragmentation and disintegration from bottom to top (Fig. 3). Quartz has some cracks but doesn't show evidence of chemical dissolution (Fig. 3). As expected, microcracks increase in number and width and evolve in a dendritic manner as weathering proceeds. These physical changes are important processes to expose fresh surfaces for chemical weathering (Scarciglia et al., 2005; Mehta, 2007) and can result in intensive intragranular microfractures which can promote each other with chemical alteration and provide pathways to transfer cations to the solute load during interaction with the flowing water (Anderson et al., 2002). In the soil samples, the reduction or even disappearance of plagioclase and K-feldspar (Fig. 4A), and significant peaks of kaolinite in the clay fraction XRD patterns (Fig. 4B) suggest that conversion of feldspar to kaolinite was the dominant chemical weathering process in the profile. Plenty of weathering resistant minerals (i.e., quartz) and weathered products (i.e., kaolinite) in the soils imply that this part underwent more intensive

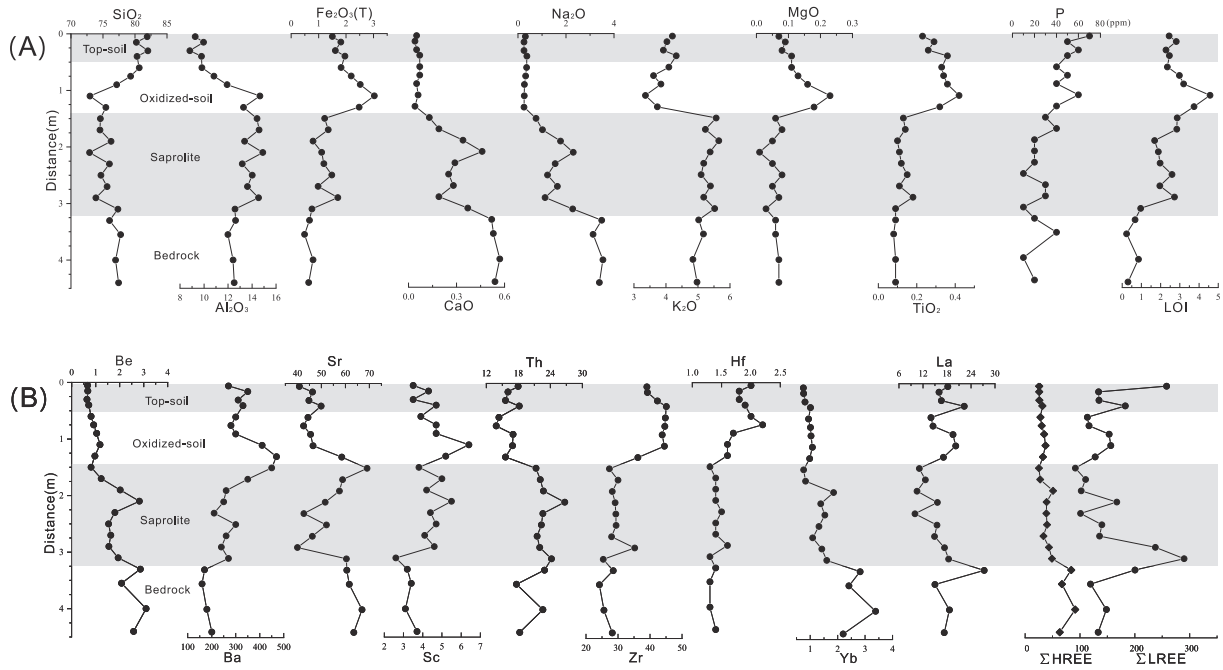

Fig. 5. (A) Vertical variations of major element compositions (in wt%) along the weathering profile. (B) Concentrations of representative trace-and rare earth element compositions (in ppm) plotted versus distance along the profile. The vertical axis means the distance below the surface of the profile. Gray and white bars divide the profile into four layers as stated in the text.

weathering than the lower profile.

We find that the CIA values are positively correlated with the LOI values (Fig. 11A). The LOI proxy is sensitive to the weathering process under humid conditions and high LOI values are commonly related to constitutional water from hydration and clay formation during weathering (Ng et al., 2001). Hence, LOI can reflect the total content of clay minerals indirectly and the highest LOI value in the bottom of the oxidized-soil layer (Fig. 5) reveals the highest clay mineral content. The LOI-clay relationship can be reinforced by Mg contents which show a positive correlation with LOI values in the oxidized-soil samples (Fig. 11E), since Mg can be inferred to be taken up by new formed clay minerals during weathering (Di Figlia et al., 2007). We contend that this phenomenon (i.e., enrichment of clay in the bottom of the oxidized-soil layer) may be attributed to leaching and downward translocation of clay minerals from the top-soil layer.

Based on mineralogical and geochemical data, a weathering trend and weathering degrees can be predicted in the Al_2O_3-CaO + Na_2O-K_2O (A-CN-K) diagram (Fig. 8). The plagioclase-free, K-feldspar-poor and kaolinite-rich soils samples (Fig. 4) are expected tend to be plotted close to the A apex in the A-CN-K diagram. However, the top-soil samples and some oxidized-soil samples cannot be plotted on the ideal weathering prediction trend and clearly demonstrate K-addition (toward to the K_2O-apex) (Fig. 8). This might be attributed to (1) the loss of Al from top-soil or (2) the significant effect on mineral release induced by plants, since roots can greatly mobilize nutrients in the rhizosphere, including Fe, K, P, etc (Zhu et al., 2014). The excessive P in the top-soil layer (Fig. 5A) is the evidence of biological pedogenesis which can result in nutrient element enrichment (Gardner et al., 1983; Dinkelaker et al., 1989).

In summary, both petrographic observation and mineralogical indices demonstrate increasing weathering degrees from bottom to top of the profile. However, The CIA, CIW and PIA values and related A-CN-K ternary plots cannot accurately reflect the weathering degrees of the top-soil and some oxidized-soil samples. We favor that this can be attributed to the influence of intensive pedogenesis which varies the physical structure and reorganize chemical element distribution patterns of the upper layers.

5.2. Evaluation of chemical element mobility

Chemical element mobilization and redistribution are very common during weathering and pedogenic processes and can be estimated by the mass transfer coefficient Tau (τ_i) (Chadwick et al., 1990; Brimhall et al., 1991). τ_i expresses the fractional mass gain or loss of an element *i* using the concentrations of the element *i* and an index element (i.e., immobile element) in both the weathered samples and parent rocks. Several elements have been considered as immobile elements during weathering and hydrothermal alteration such as Al (Ji et al., 2000; Das and Krishnaswami, 2007), Ti (Nesbitt and Markovics, 1997; Braun et al., 2009), Nb and Ta (Brimhall and Dietrich, 1987; Little and Aeolus Lee, 2006), Zr and Hf (Riebe et al., 2003; Hastie et al., 2008), Th (Braun et al., 1998; Ndjigui et al., 2008) and Sc (Shotyk et al., 2001). In this study, Zr is selected as the immobile element. The calculation of τ_i is $\tau_i = [(i_{sample} \times Zr_{bedrock})/(i_{bedrock} \times Zr_{sample})\text{-}1]$, where $Zr_{bedrock}$ in this study is an average value of the bottom two bedrock samples. Then, a positive τ value indicates a gain of the element, a τ value close to zero implies no loss or gain, whereas a negative τ value indicates that the element is lost during weathering and τ values close to −1 means almost 100% chemical depletion during weathering.

The τ values of selected elements are shown in Figs. 9 and 10. Major elements Ca and Na decrease significantly with decreasing depth (Figs. 5, 9), suggesting that these two elements were vulnerable and easily leached during weathering and pedogenic processes. The contents of K and P in top-soil samples are slightly higher than those in oxidized-soil samples (Figs. 5, 10). It may be relevant to the effects of plant roots and biogeochemical processes in the top-soil (Weber et al., 2006; Zhu et al., 2014), as plant roots develop only in the top-soil layer and rarely reach the oxidized-soil layer. It is worth noting that the contents of Ti and Zr in top-soil samples are slightly lower than those in oxidized-soil samples (Fig. 5), implying low contents of chemically stable accessory minerals (such as zircon and titanite) in the top-soil samples. Some large ion lithophile elements (LILEs), e.g., Rb, Sr and Th and high field strength elements (HFSEs), e.g., Nb and Ta have the τ values around −0.5 for the soil layers, however, they have τ values around 0 for the saprolite layer (Fig. 9). This suggests that these LILEs and HFSEs were

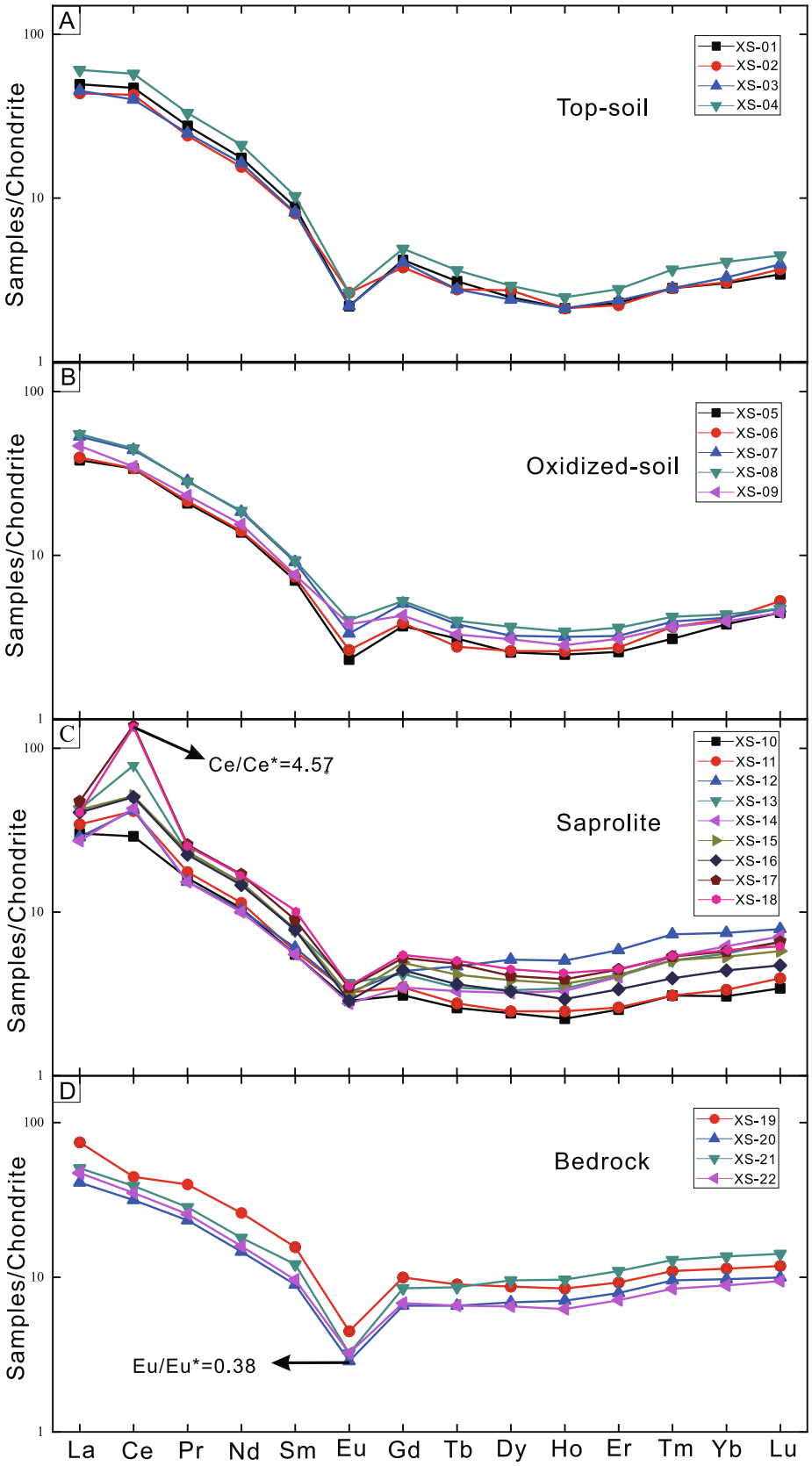

Fig. 6. Chondrite-normalized REE patterns of all the analyzed samples. Note that all sample show negative Eu anomaly and saprolite samples have distinct positive Ce anomalies. Compositions of the CI carbonaceous chondrite (Taylor and McLennan, 1985) were employed for the normalization. Eu- and Ce-anomaly calculated as $Eu/Eu^* = Eu_N/(Sm_N \times Gd_N)^{1/2}$ and $Ce/Ce^* = Ce_N/(La_N \times Pr_N)^{1/2}$, respectively.

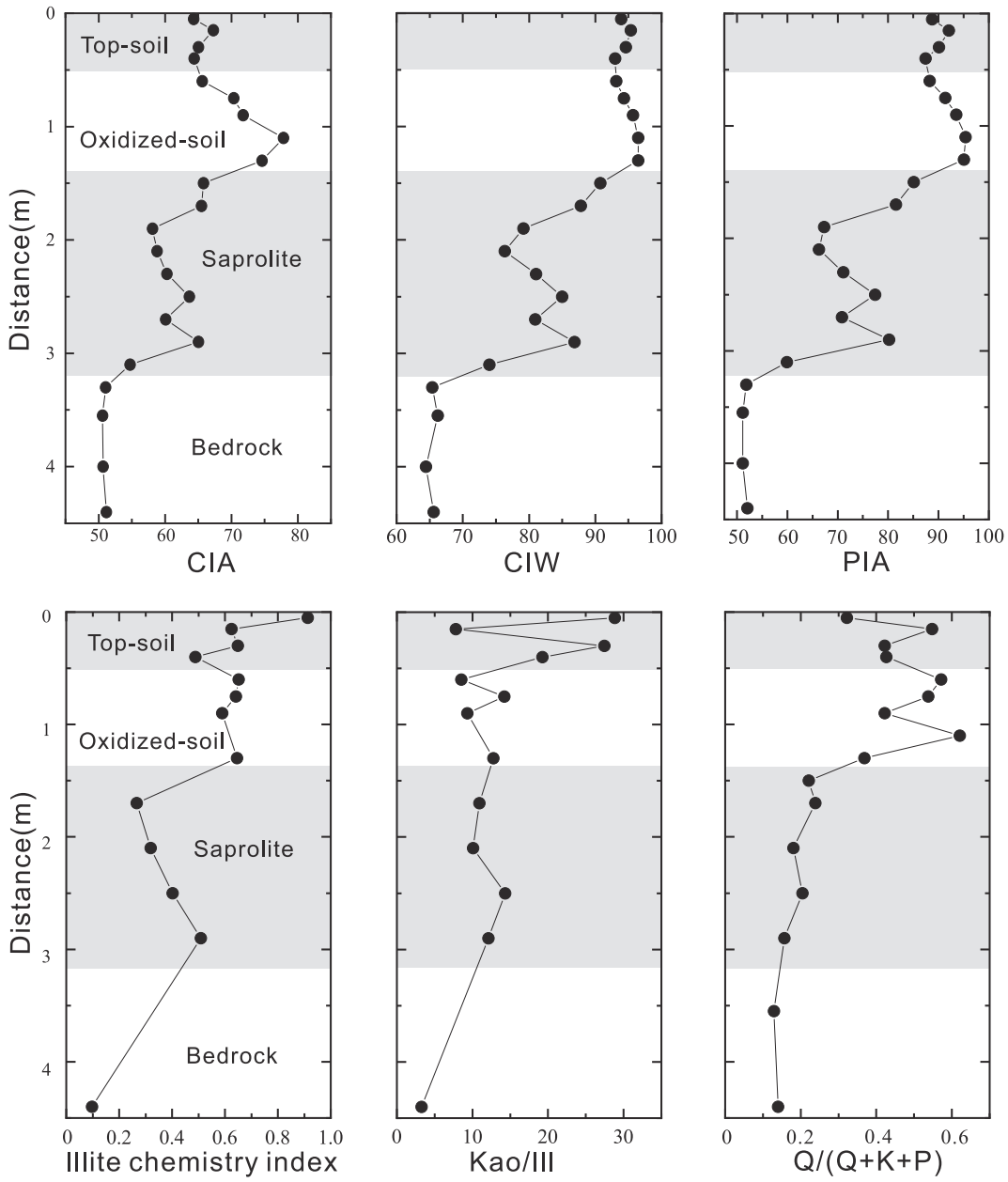

Fig. 7. Vertical plots of the weathering indices of the studied profile. The Kao/Ill and Q/(Q + K + P) values were based on XRD analysis data. For the CIA, CIW and PIA calculations, see the related sentences in the main text. Q: quartz, P: plagioclase, K: K-feldspar, Kao: kaolinite, Ill: illite.

less mobile during moderate weathering alteration but were easily lost in the intensive weathering alteration or in the pedogenic process.

The behaviors of REEs can be effectively used to understand weathering dynamics (Rajamani et al., 2009). In this study, heavy rare earth elements (HREEs) were more efficiently leached than light rare earth elements (LREEs) when weathering and pedogenesis were incipient (Fig. 9), because kaolinite and illite rich residual material could acquire LREE enriched pattern (Nesbitt, 1979; Rajamani et al., 2009). Weathered samples have roughly similar REE patterns with the fresh bedrock sample except Ce (Fig. 6). Ce^{3+} is soluble, but Ce commonly becomes insoluble and highly adsorptive when it is oxidized to CeO_2 on Fe/Mn (hydro)oxides coatings in oxic environments (Braun et al., 1990; Bao and Zhao, 2008; Jian et al., 2019). Hence, positive Ce anomaly is most likely to occur in the upper part of weathering profile (Laufer et al., 1984). Note that Ce is not well related to Fe/Mn oxides in our investigated profile (Fig. 11F) and the oxidized-soil samples have the highest Fe/Mn oxide content (Fig. 11F). Therefore, why the most positive Ce anomalies are present in some saprolite samples remains unclear and deserves more attention in future study. Furthermore, the depletion of Eu in the weathering samples (Fig. 6) may attribute to chemical weathering of Eu-bearing plagioclase feldspars in the parent rocks (Condie et al., 1995).

5.3. *Controls on physical and chemical alterations during bedrock weathering and soil development*

To a great extent, weathering and pedogenesis on the Earth's surface can be collectively governed by climatic (e.g., temperature, precipitation and runoff), tectonic (e.g., relief, uplift, exhumation and physical erosion), biogeochemical (e.g., the influence of organisms during soil development) and internally lithological (e.g., ultramafic, mafic, felsic and their texture and structure) factors over various geological timescales (e.g., Raymo and Ruddiman, 1992; Bluth and Kump, 1994; Riebe et al., 2001; Jacobson et al., 2003; Jobbágy and Jackson, 2004; West

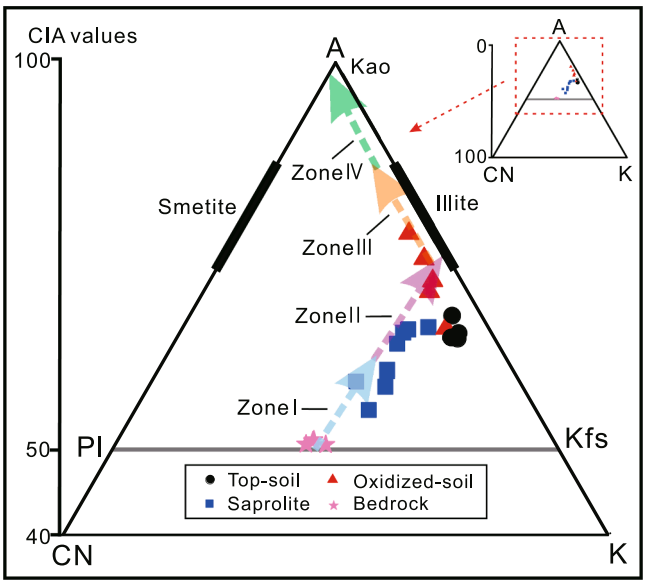

Fig. 8. The Al_2O_3-(CaO^*+Na_2O)-K_2O (A-CN-K) ternary diagram for the analyzed samples. Oxides are in moles and CaO^* represents Ca in silicate-bearing minerals only. The colored lines with arrows show predicted weathering trends, modified from Jian et al. (2019). Zones I, II, III, IV were on behalf of the bedrock, saprolite, oxidized-soil and top-soil samples based on their bulk and clay fraction XRD analysis results respectively. Note that the top-soil samples and some oxidized-soil samples show different illustrations based on mineralogical and elemental geochemical data. Kao: kaolinite, Pl: plagioclase, Kfs: K-feldspar.

et al.,2005; Egli et al., 2008; Vitousek et al., 2010; Dixon et al., 2012; Jian et al., 2019). Our results indicate that weathering and pedogenic processes can result in different physicochemical changes on bedrock and thus show differential physical and chemical behaviors in regolith profiles.

The saprolite is produced from parent bedrock by chemical dissolution and mineral transformation. This process is commonly within a system in which the weathering residues are left in place. Alteration degrees always depend on the chemical dissolution conditions, such as temperature, moisture and hydraulic conductivity. In this case, humid tropical and subtropical regions tend to have intensive chemical weathering intensity and saprolite therein commonly display relatively high mineralogical and geochemical weathering index values (Rajamani et al., 2009; Su et al., 2015; Liu et al., 2016; Fang et al., 2019).

In contrast to the formation of saprolite, soil development occurs within a more open system because soils are easily in contact with various spheres of the Earth's surface. Similar to the weathering process, temperature and moisture can influence soil properties during the pedogenic process by affecting type and rates of chemical, biological, and physical alterations (Dahlgren et al., 1997; Birkeland, 1999). Soil production will decrease with depth, which is related to the exponential decrease of temperature amplitude with depth, the reduction in water penetration, and possibly a reduced bioturbation activity (Minasny et al., 2015). Chemical and biophysical alterations in soils are not volumetric in most cases, i.e., an elementary volume may dilate or collapse during soil evolution (Egli and Fitze, 2000; Egli et al., 2001). Therefore, elutriation caused by rainfall, vertical migration of meteoric water and translocation of solid materials might take place due to the loose and porous media, especially for soils in high precipitation regions. High precipitation, especially short-term extreme rainfall can lead to high leaching rates of elements from soils (Egli et al., 2003; Dahms et al., 2012). Podzolization and lessivage are commonly observed under these conditions, which can redistribute clay and organic matter to subsoils (Phillips, 2019). This is why the bottom of the oxidized-soil layer has the highest clay content. Downward migration of clay and organic matter from the surface to deeper horizons can influence Al, Fe, K, Ca, Na and Mg content (Bravard and Righi, 1990; Martz and de Jong, 1990; Jansen et al., 2003; Horbe et al., 2004; Nascimento et al., 2004; Brantley and White, 2009; Tadini et al., 2018; Souza et al., 2018), and consequently, the geochemical weathering proxies, such as CIA.

Biological process is also a noticeable factor in redistribution of elements in soils, which might lead to compositional heterogeneity (Minasny et al., 2015) and results in the obvious enrichment of P and K in soils (Fig. 5). As a result, the mobile element-based geochemical indices (e.g., CIA), which indicate different variation trends from the mineralogical indices, mislead the chemical weathering intensity evaluations for the soil samples (Fig. 7, Fig. 11). The boundary zone between soils and saprolite can be described as a system made up of closed or partly open microenvironments (Tardy et al. 1973; Tardy, 1997). The effect of pedogenesis decreases with depth on a profile and ceases at the bottom of the oxidized-soil layer. The increasing porosity and decreasing coherence make the bottom of oxidized-soil layer become a transition zone where material accumulates after vertical translocation from the top-soil layer.

Physical erosion induced by tectonic activity also plays an important role in weathering and pedogenesis. Physical erosion provides fresh mineral surfaces for soil formation and chemical weathering reactions. In tectonically active regions, chemical weathering reactions sometimes are kinetically limited because the reaction rates cannot compare favorably with supply rates of fresh minerals (West et al., 2005; Mavris et al., 2010). Kinetically limited weathering type results in undeveloped weathering regolith and relatively low chemical weathering intensity. Note that the study area is located in a relatively tectonically stable region (Jian et al., 2020a). Hence, soils and regolith profiles in this area are relatively thick (Su et al., 2015; Liu et al., 2016). Similarly, pedogenesis and chemical weathering can assist erosion through dissolution of primary minerals, thereby reducing bedrock coherence and resistance to physical disruption. These coupling processes have led some to suggest that physical erosion exerts a strong control on development of regolith profiles (Riebe et al., 2001; von Blanckenburg et al., 2004).

5.4. Implications

Material transfer (including physical, chemical and biological) process in the Critical Zone on the Earth's surface is a hot topic in geoscience studies (Brantley et al., 2007; Richter and Mobley, 2009; Jin et al., 2010; Brantley and Lebedeva, 2011; Buss et al., 2017; Li et al., 2017). As the fast development of different kinds of mass spectrum techniques in past decades, a growing number of elemental and isotopic (such as non-traditional isotopes) tracers have been used in characterizing weathering processes on regolith profiles in the Critical Zone (e.g., Pistiner and Henderson, 2003; Liu et al., 2013; Wimpenny et al., 2014; Brewer et al., 2018; Chen et al., 2020; Li et al., 2021). The results in this study underline the differential physical and chemical behaviors during the weathering and pedogenic processes, especially in those high precipitation and tectonically stable regions. This means that the material transfer process is quite complicated in different layers of regolith profiles and caution should be exercised while using those novel tracers to characterize the in-situ weathering process on regolith profiles. Accurately evaluating chemical weathering degrees of the profiles using traditional indicators are highly recommended before applications of new tracers.

The major element-based CIA proxy (and related proxies) and the A-CN-K diagram have been widely used in chemical weathering intensity investigations on regolith, siliciclastic sediments and sedimentary rocks (e.g., Nesbitt and Markovics, 1997; Young and Nesbitt, 1998; Buggle et al., 2011; Jian et al., 2013, 2019; Sharma et al., 2013; Thorpe et al., 2019; Thorpe and Hurowitz, 2020). However, as shown in this study, weathering degrees of soils may be underestimated when using CIA values because of the possible vertical translocation of fine-grained weathering products and the occurrence of K biological uptake

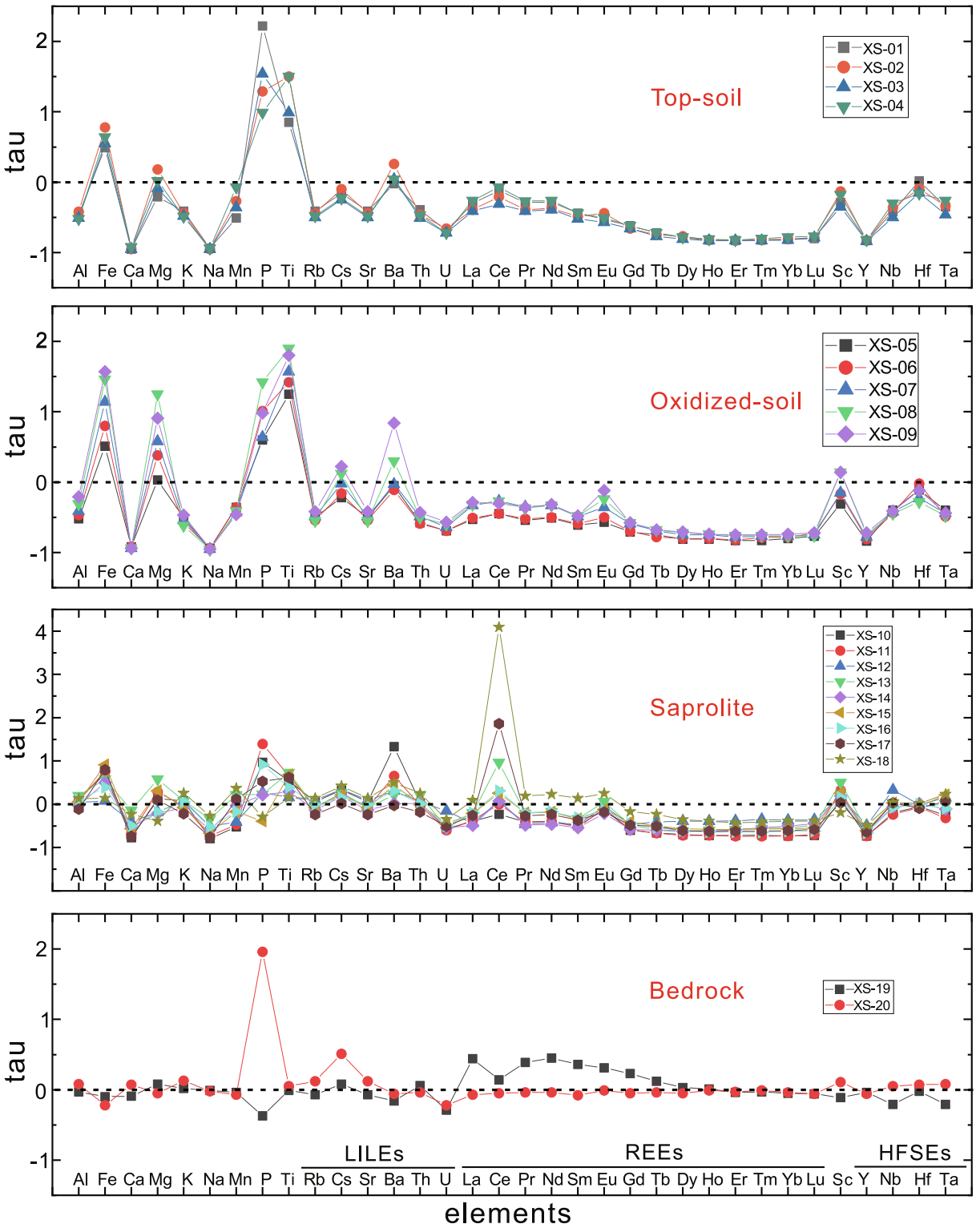

Fig. 9. Plots of Tau values of the major and trace elements. For calculation details, see the related sentences in the main text. LILEs: large ion lithophile elements; REEs: rare earth elements; HFSEs: high field strength elements.

(Fig. 12). Chemical weathering evaluation of sediment source terrains and regions where sediments are transported can also be misdirected if the siliciclastic sediments are contributed by erosion of these kinds of soils. Therefore, other indicators, such as petrographic and mineralogical proxies, are also important to better understanding weathering processes and related physical and chemical alterations during the formation of regolith and sediments on the Earth' surface. The findings in this study also suggest that a dynamic sediment source might be present in high-rainfall regions with highly developed soils for a sediment source-to-sink system.

6. Conclusions

This study presents an integrated investigation on a subtropical

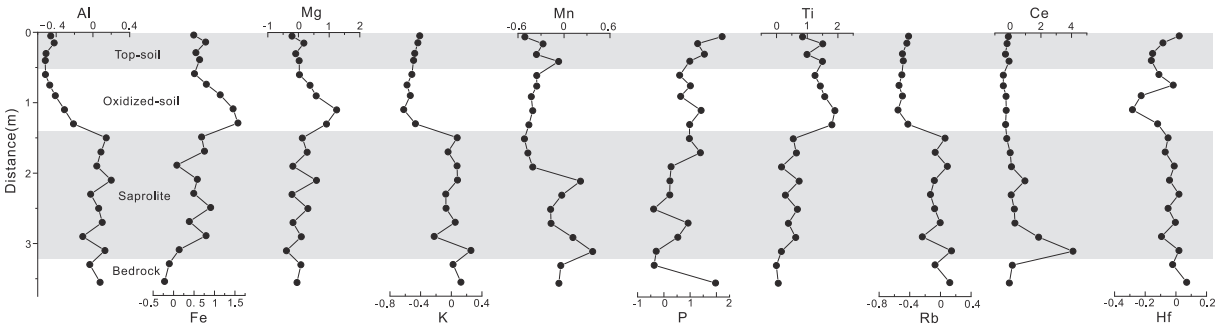

Fig. 10. Vertical variations of the Tau values of selected elements along the weathering profile.

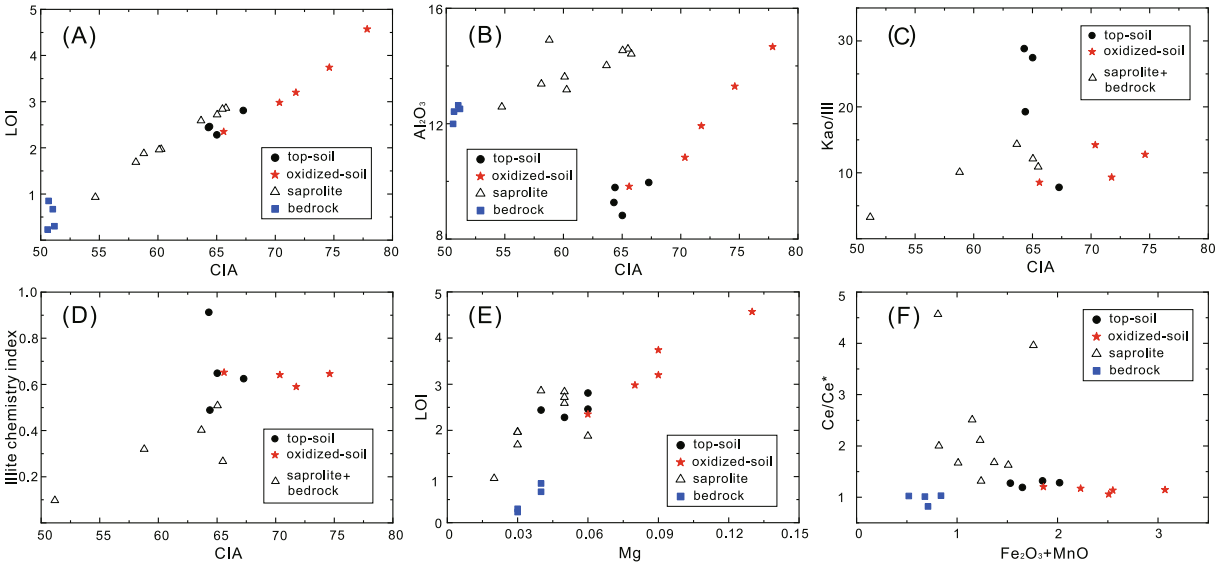

Fig. 11. Binary diagrams among element compositions (in wt%), clay mineral proxy values and CIA values. (A): CIA values vs. LOI values; (B): CIA values vs. Al_2O_3 contents; (C): CIA values vs. Kao/Ill values; (D): CIA values vs. Illite chemistry index values; (E): Magnesium contents vs. LOI values; (F): Fe_2O_3 + MnO contents vs. Ce-anomaly values, note that the Ce-anomalies are not well related to the Fe/Mn oxides contents.

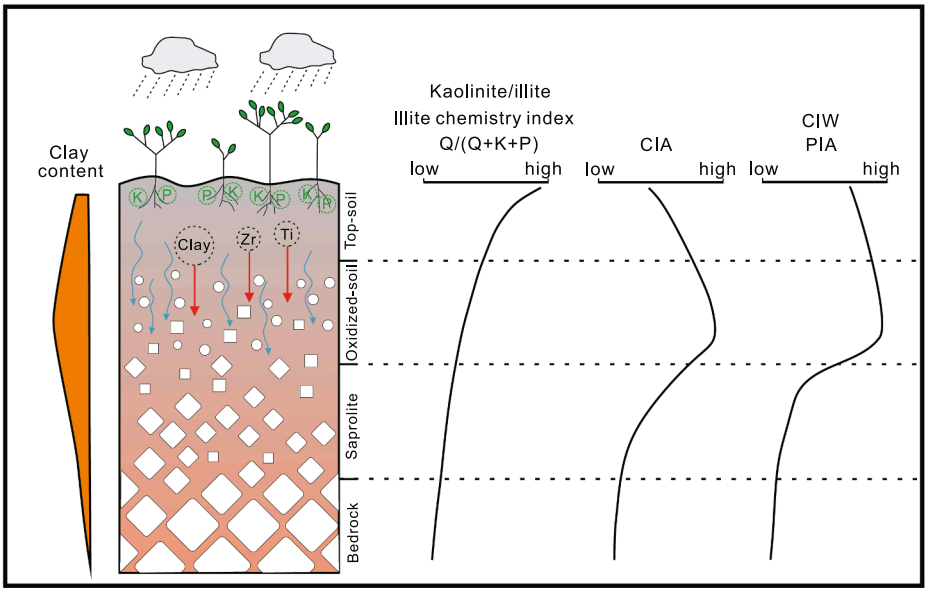

Fig. 12. A schematic diagram showing major physical, chemical and biological behaviors on a granitic regolith profile under subtropical high-rainfall and tectonically stable conditions. Vertical leaching and translocation of clay in soils can influence CIA, CIW and PIA values and thus the weathering intensity of soils might be underestimated. The K-uptake by plant roots can also result in lower CIA values in the top-soil layer. Petrographic and mineralogical proxies such as kaolinite/illite, illite chemistry index, and quartz/(quartz + K-feldspar + plagioclase), to some extent, can more accurately reflect weathering intensity than those geochemical proxies. Red arrows indicate the direction of migration, light blue arrows indicate the migration channels of loose and porous top-soil. K: potassium, P: phosphorus, Zr: zirconium, Ti: titanium. (For interpretation of the references to colour in this figure legend, the reader is referred to the web version of this article.)

granitic regolith profile in SE China by using petrography, mineralogy and elemental geochemistry and yields the following conclusions:

1) Petrographic and mineralogical results indicate that the profile has experienced intensive physical and chemical weathering alterations, and conversion of feldspar (both plagioclase and K-feldspar) to kaolinite is the dominant mineral transformation process on the profile.
2) Geochemical results demonstrate that the elements Al, Ti, Zr and Hf, which are previously thought as chemically immobile elements on a profile scale, are depleted in top-soil samples. This is probably attributed to intensive vertical leaching and translocation of fine-grained solid materials (such as zircon and clay minerals) through the top-soil and oxidized-soil layers, since heavy rain frequently happens in the study area. Furthermore, the enrichment of K and P in top-soil samples is most likely due to biological process.
3) Our findings reveal the differential physical and chemical behaviors of the regolith profile between weathering and pedogenesis. The chemical weathering intensity of the soils may be underestimated when using the traditional geochemical indicators, such as the CIA proxy and the A-CN-K ternary diagram, especially for those tropical–subtropical, tectonically stable, high precipitation regions. Petrographic and mineralogical proxies are also important to accurately evaluate the chemical weathering degrees of the regolith profiles. The CIA values can be a baseline that further interpretations are needed to accompany such values.

Declaration of Competing Interest

The authors declare that they have no known competing financial interests or personal relationships that could have appeared to influence the work reported in this paper.

Acknowledgments

This work was supported by the National Natural Science Foundation of China (Nos. 41902126, 41806052), Natural Science Foundation of Fujian Province (No. 2017J05067), Xiamen University Fundamental Research Funds for the Central Universities (Nos. 20720190097, 20720190103). We would like to thank Hanghai Liang and Dongming Hong of Xiamen University for their contributions to sample collection and lab work. We are grateful to Michael T. Thorpe and other two anonymous reviewers for their thoughtful reviews that improved this manuscript.

Appendix A. Supplementary data

Supplementary data to this article can be found online at https://doi.org/10.1016/j.catena.2021.105368.

References

Anderson, S.P., Dietrich, W.E., Brimhall Jr, G.H., 2002. Weathering profiles, mass-balance analysis, and rates of solute loss: linkages between weathering and erosion in a small, steep catchment. Geol. Soc. America Bull. 114 (9), 1143–1158. https://doi.org/10.1130/0016-7606(2002)114<1143:WPMBAA>2.0.CO;2.

Andò, S., Garzanti, E., Padoan, M., Limonta, M., 2012. Corrosion of heavy minerals during weathering and diagenesis: a catalog for optical analysis. Sed. Geol. 280, 165–178. https://doi.org/10.1016/j.sedgeo.2012.03.023.

Bao, Z., Zhao, Z., 2008. Geochemistry of mineralization with exchangeable REY in the weathering crusts of granitic rocks in South China. Ore Geol. Rev. 33 (3–4), 519–535. https://doi.org/10.1016/j.oregeorev.2007.03.005.

Berner, R.A., 1995. Chemical weathering and its effect on atmospheric CO2 and climate. Mineral. Soc. America 31, 565–583. https://doi.org/10.1515/9781501509650-015.

Birkeland, P.W., 1999. Soils and Geomorphology. Oxford University Press, New York.

Biscaye, P.E., 1965. Mineralogy and sedimentation of recent deep-sea clay in the Atlantic Ocean and adjacent seas and oceans. Geol. Soc. Am. Bull. 76, 803–832. https://doi.org/10.1130/0016-7606(1965)76[803:MASORD]2.0.CO;2.

Blum, J.D., Erel, Y., 1997. Rb–Sr isotope systematics of a granitic soil chronosequence: the importance of biotite weathering. Geochim. Cosmochim. Acta 15, 3193–3204. https://doi.org/10.1016/S0016-7037(97)00148-8.

Bluth, G.J., Kump, L.R., 1994. Lithologic and climatologic controls of river chemistry. Geochim. Cosmochim. Acta 58, 341–2359. https://doi.org/10.1016/0016-7037(94)90015-9.

Bouchez, J., Gaillardet, J., 2014. How accurate are rivers as gauges of chemical denudation of the Earth surface? Geology 42, 171–174. https://doi.org/10.1130/G34934.1.

Brady, N.C., Weil, R.R., 2008. The nature and properties of soils. Prentice Hall, Upper Saddle River, NJ.

Braga, M.S., Paquet, H., Begonha, A., 2002. Weathering of granites in a temperate climate (NW Portugal): granitic saprolites and arenization. Catena 49 (1–2), 41–56. https://doi.org/10.1016/S0341-8162(02)00017-6.

Brantley, S.L., White, A.F., 2009. Approaches to modeling weathered regolith. Rev. Mineral. Geochem. 70, 435–484. https://doi.org/10.2138/rmg.2009.70.10.

Brantley, S.L., Goldhaber, M.B., Ragnarsdottir, K.V., 2007. Crossing disciplines and scales to understand the critical zone. Elements 3(5), 307–314. https://doi.org/307-314. 10.2113/gselements.3.5.307.

Brantley, S.L., 2008. Understanding soil time. Science 321, 1454–1455. https://doi.org/10.1126/science.1161132.

Brantley, S.L., Lebedeva, M., 2011. Learning to read the chemistry of regolith to understand the Critical Zone. Annu. Rev. Earth Planet. Sci. 39, 387–416. https://doi.org/10.1146/annurev-earth-040809-152321.

Braun, J.J., Pagel, M., Muller, J.P., Michard, A., Guillet, B., 1990. Cerium anomalies in lateritic profiles. Geochim. Cosmochim. Acta 54, 781–795. https://doi.org/10.1016/0016-7037(90)90373-S.

Braun, J.-J., Descloitres, M., Riotte, J., Fleury, S., Barbiéro, L., Boeglin, J.-L., Violette, A., Lacarce, E., Ruiz, L., Sekhar, M., Mohan Kumar, M.S., Subramanian, S., Dupré, B., 2009. Regolith mass balance inferred from combined mineralogical, geochemical and geophysical studies: Mule Hole gneissic watershed, South India. Geochim. Cosmochim. Acta 73, 935–961. https://doi.org/10.1016/j.gca.2008.11.013.

Braun, J.-J., Viers, J., Dupré, B., Polve, M., Ndam, J., Muller, J.-P., 1998. Solid/liquid REE fractionation in the lateric system of Goyoum, East Cameroon: the implication for the present dynamics of the soil covers of the humid tropical regions. Geochim. Cosmochim. Acta 62, 273–299. https://doi.org/10.1016/s0016-7037(97)00344-x.

Bravard, S., Righi, D., 1990. Podzols in Amazonia. Catena 17, 461–475. https://doi.org/10.1016/0341-8162(90)90046-G.

Brewer, A., Teng, F.Z., Dethier, D., 2018. Magnesium isotope fractionation during granite weathering. Chem. Geol. 501, 95–103. https://doi.org/10.1016/j.chemgeo.2018.10.013.

Brimhall, G.H., Dietrich, W.F., 1987. Constitutive mass balance relations between chemical composition, volume, density, porosity and strain in metasomatic hydrothermal systems: results on weathering pedogenesis. Geochim. Cosmochim. Acta 51, 567–587. https://doi.org/10.1016/0016-7037(87)90070-6.

Brimhall, G.H., Lewis, C.L., Ford, C., Bratt, J., Taylor, G., Warin, O., 1991. Quantinative geochemical approach to pedogenesis: importance of parent material reduction, volumetric expansion, and eolian influx in lateritization. Geoderma 51, 51–91. https://doi.org/10.1016/0016-7061(91)90066-3.

Buggle, B., Glaser, B., Hambach, U., Gerasimenko, N., Marković, S., 2011. An evaluation of geochemical weathering indices in loess–paleosol studies. Quat. Int. 240 (1–2), 12–21. https://doi.org/10.1016/j.quaint.2010.07.019.

Buss, H.L., Lara, M.C., Moore, O.W., Kurtz, A.C., Schulz, M.S., White, A.F., 2017. Lithological influences on contemporary and long-term regolith weathering at the Luquillo Critical Zone Observatory. Geochim. Cosmochim. Acta 196, 224–251. https://doi.org/10.1016/j.gca.2016.09.038.

Campodonico, V.A., Martínez, J.O., Verdecchia, S.O., Pasquini, A.I., Depetris, P.J., 2014. Weathering assessment in the Achala Batholith of the Sierra de Comechingones, Córdoba, central Argentina. I: Granite–regolith Fractionation. Catena 123, 121–134. https://doi.org/10.1016/j.catena.2014.07.016.

Chadwick, O.A., Brimhall, G.H., Hendricks, D.M., 1990. From a black to a fray box: a mass balance interpretation of pedogenesis. Geomorphology 3, 369–390. https://doi.org/10.1016/0169-555X(90)90012-F.

Chamley, H., 1989. Clay formation through weathering. In Clay sedimentology. Springer, Berlin, Heidelberg.

Chen, H., Liu, X.M., Wang, K., 2020. Potassium isotope fractionation during chemical weathering of basalts. Earth Planet. Sci. Lett. 539, 116192. https://doi.org/10.1016/j.epsl.2020.116192.

Clift, P.D., Wan, S., Blusztajn, J., 2014. Reconstructing chemical weathering, physical erosion and monsoon intensity since 25 Ma in the northern South China Sea: a review of competing proxies. Earth Sci. Rev. 130, 86–102. https://doi.org/10.1016/j.earscirev.2014.01.002.

Condie, K.C., Dengate, J., Cullers, R.L., 1995. Behavior of rare earth elements in a palaeoweathering profile on granodiorite in the Front Range, Colorado, USA. Geochim. Cosmochim. Acta 59, 279–294. https://doi.org/10.1016/0016-7037(94)00280-Y.

Dahlgren, R.A., Boettinger, J.L., Huntington, G.L., Amundson, R.G., 1997. Soil development along an elevational transect in the western Sierra Nevada, California. Geoderma 78, 207–236. https://doi.org/10.1016/S0016-7061(97)00034-7.

Dahms, D., Favilli, F., Krebs, R., Egli, M., 2012. Soil weathering and accumulation rates of oxalate-extractable phases derived from alpine chronosequences of up to 1 Ma in age. Geomorphology 151, 99–113. https://doi.org/10.1016/j.geomorph.2012.01.021.

Das, A., Krishnaswami, S., 2007. Elemental geochemistry of river sediments from the Deccan Traps, India: implications to sources of elements and their mobility during

basalt–water interaction. Chem. Geol. 242, 232–254. https://doi.org/10.1016/j.chemgeo.2007.03.023.
Dessert, C., Dupré, B., Gaillardet, J., François, L.M., Allègre, C.J., 2003. Basalt weathering laws and the impact of basalt weathering on the global carbon cycle. Chem. Geol. 202, 257–273. https://doi.org/10.1016/j.chemgeo.2002.10.001.
Di Figlia, M.G., Bellanca, A., Neri, R., Stefansson, A., 2007. Chemical weathering of volcanic rocks at the island of Pantelleria, Italy: information from soil profile and soil solution investigations. Chem. Geol. 246 (1–2), 1–18. https://doi.org/10.1016/j.chemgeo.2007.07.025.
Dickinson, W.R., 1985. Interpreting provenance relations from detrital modes of sandstones. Provenance of arenites 333–361. https://doi.org/10.1007/978-94-017-2809-6_15.
Dinkelaker, B., Romheld, V., Marschner, H., 1989. Citric acid excretion and precipitation of calcium citrate in the rhizosphere of white lupin (Lupinus albus L.). Plant Cell Environ. 12, 285–292. https://doi.org/10.1111/j.1365-3040.1989.tb01942.x.
Dixon, J.L., Hartshorn, A.S., Heimsath, A.M., DiBiase, R.A., Whipple, K.X., 2012. Chemical weathering response to tectonic forcing: a soils perspective from the San Gabriel Mountains, California. Earth Planet. Sci. Lett. 323, 40–49. https://doi.org/10.1016/j.epsl.2012.01.010.
Dosseto, A., Turner, S.P., Chappell, J., 2008. The evolution of weathering profiles through time: new insights from uranium-series isotopes. Earth Planet. Sci. Lett. 274 (3–4), 359–371. https://doi.org/10.1016/j.epsl.2008.07.050.
Egli, M., Fitze, P., 2000. Formulation of pedologic mass balance based on immobile elements: a revision. Soil Sci. 165, 437–443. https://doi.org/10.1097/00010694-200005000-00008.
Egli, M., Mirabella, A., Fitze, P., 2001. Weathering and evolution of soils formed on granitic, glacial deposits: results from chronosequences of Swiss alpine environments. Catena 45, 19–47. https://doi.org/10.1016/S0341-8162(01)00138-2.
Egli, M., Mirabella, A., Fitze, P., 2003. Formation rates of smectites derived from two Holocene chronosequences in the Swiss Alps. Geoderma 117, 81–98. https://doi.org/10.1016/S0016-7061(03)00136-8.
Egli, M., Mirabella, A., Sartori, G., 2008. The role of climate and vegetation in weathering and clay mineral formation in late Quaternary soils of the Swiss and Italian Alps. Geomorphology 102 (3–4), 307–324. https://doi.org/10.1016/j.geomorph.2008.04.001.
Esquevin, J., 1969. Influence de la composition chimique des illites sur leur cristallinité. Bull. Centre Rech. Pau-SNPA 3 (1), 147–153. http://pascal-francis.inist.fr/vibad/index.php?action=getRecordDetail&idt=GEODEBRGM6901019346.
Fang, Q., Hong, H., Furnes, H., Chorover, J., Luo, Q., Zhao, L., Algeo, T.J., 2019. Surficial weathering of kaolin regolith in a subtropical climate: implications for supergene pedogenesis and bedrock argillization. Geoderma 337, 225–237. https://doi.org/10.1016/j.geoderma.2018.09.020.
Fedo, C.M., McGlynn, I.O., McSween, H.Y., 2015. Grain size and hydrodynamic sorting controls on the composition of basaltic sediments: implications for interpreting martian soils. Earth Planet. Sci. Lett. 423, 67–77. https://doi.org/10.1016/j.epsl.2015.03.052.
Fedo, C.M., Nesbitt, H.W., Young, G.M., 1995. Unraveling the effects of potassium metasomatism in sedimentary rocks and paleosols, with implications for paleo-weathering conditions and provenance. Geology 23, 921–924 https://doi.org/0.1130/0091-7613(1995)0232.3.CO;2.
Gaillardet, J., Dupré, B., Louvat, P., Alle ‘gre, C.J., 1999. Global silicate weathering and CO2 consumption rates deduced from the chemistry of the large rivers. Chem. Geol. 159, 3–30. https://doi.org/10.1016/S0009-2541(99)00031-5.
Gardner, W.K., Barber, D.A., Parbery, D.G., 1983. The acquisition of phosphorus by Lupinus albus L. III. The probable mechanism by which phosphorus movement in the soil/root interface is enhanced. Plant Soil 70, 107–124. https://doi.org/10.1007/BF02374894.
Goddéris, Y., Donnadieu, Y., Tombozafy, M., Dessert, C., 2008. Shield effect on continental weathering: implication for climatic evolution of the Earth at the geological time-scale. Geoderma 145 (3–4), 439–448. https://doi.org/10.1016/j.geoderma.2008.01.020.
Harnois, L., 1988. The CIW index—a new chemical index of weathering. Sed. Geol. 55, 319–322. https://doi.org/10.1016/0037-0738(88)90137-6.
Hastie, A.R., Kerr, A.C., Mitchell, S.F., Millar, I.L., 2008. Geochemistry and petrogenesis of Cretaceous oceanic plateau lavas in eastern Jamaica. Lithos 101, 323–343. https://doi.org/10.1016/j.lithos.2007.08.003.
He, M., Zheng, H., Huang, X., Jia, J., Li, L., 2013. Yangtze River sediments from source to sink traced with clay mineralogy. J. Asian Earth Sci. 69, 60–69. https://doi.org/10.1016/j.jseaes.2012.10.001.
Heimsath, A.M., Dietrich, W.E., Nishiizumi, K., Finkel, R.C., 1997. The soil production function and landscape equilibrium. Nature 388, 358–361. https://doi.org/10.1038/41056.
Hodell, D.A., Mead, G.A., Mueller, P.A., 1990. Variation in the strontium isotopic composition of seawater (8 Ma to present): implications for chemical weathering rates and dissolved fluxes to the oceans. Chem. Geol. 80, 291–307. https://doi.org/10.1016/0168-9622(90)90011-Z.
Horbe, A.M.C., Horbe, M.A., Suguio, K., 2004. Tropical Spodosols in northeastern Amazonas State, Brazil. Geoderma 119, 55–68. https://doi.org/10.1016/S0016-7061(03)00233-7.
Irfan, T.Y., Dearman, W.R., 1978. The engineering petrography of a weathered granite in cornwall, england. Q. J. Eng. Geol. Hydrogeol. 11 (3), 233–244. https://doi.org/10.1144/GSL.QJEG.1978.011.03.03.
Jacobson, A.D., Blum, J.D., Chamberlain, C.P., Craw, D., Koons, P.O., 2003. Climatic and tectonic controls on chemical weathering in the New Zealand southern Alps. Geochim. Cosmochim. Acta 67, 29–46. https://doi.org/10.1016/S0016-7037(02)01053-0.
Jansen, B., Nierop, K.G.J., Verstraten, J.M., 2003. Mobility of Fe(II), Fe(III) and Al in acidic forest soils mediated by dissolved organic matter: Influence of solution pH and metal/organic carbon ratios. Geoderma 113, 323–340. https://doi.org/10.1016/S0016-7061(02)00368-3.
Ji, H., Ouyang, Z., Wang, S., Zhou, D., 2000. Element geochemistry of weathering profile of dolomitite and its applications for the average chemical composition of the upper-continental crust. Sci. China (Series D) 43, 23–35. https://doi.org/10.1007/BF02877828.
Jian, X., Guan, P., Zhang, W., Feng, F., 2013. Geochemistry of Mesozoic and Cenozoic sediments in the northern Qaidam basin, northeastern Tibetan Plateau: implications for provenance and weathering. Chem. Geol. 360, 74–88. https://doi.org/10.1016/j.chemgeo.2013.10.011.
Jian, X., Yang, S., Hong, D., Liang, H., Zhang, S., Fu, H., Zhang, W., 2020a. Seasonal geochemical heterogeneity of sediments from a subtropical mountainous river in SE China. Mar. Geol. 422, 106120. https://doi.org/10.1016/j.margeo.2020.106120.
Jian, X., Zhang, W., Liang, H., Guan, P., Fu, L., 2019. Mineralogy, petrography and geochemistry of an early Eocene weathering profile on basement granodiorite of Qaidam basin, northern Tibet: tectonic and paleoclimatic implications. Catena 172, 54–64. https://doi.org/10.1016/j.catena.2018.07.029.
Jian, X., Zhang, W., Yang, S., Kao, S.J., 2020a. Climate-dependent sediment composition and transport of mountainous rivers in tectonically stable, subtropical East Asia. Geophys. Res. Lett. 47(3), e2019GL086150. https://doi.org/10.1029/2019GL086150.
Jin, L., Ravella, R., Ketchum, B., Bierman, P.R., Heaney, P., White, T., Brantley, S.L., 2010. Mineral weathering and elemental transport during hillslope evolution at the Susquehanna/Shale Hills Critical Zone Observatory. Geochim. Cosmochim. Acta 74 (13), 3669–3691. https://doi.org/10.1016/j.gca.2010.03.036.
Jobbágy, E.G., Jackson, R.B., 2004. The uplift of soil nutrients by plants: biogeochemical consequences across scales. Ecology 85 (9), 2380–2389. https://doi.org/10.1890/03-0245.
Kabata-Pendias, A., Pendias, H., 2001. Trace Elements in Soils and Plants. CRV Press, Boca Raton, Florida.
Kretzschmar, R., Robarge, W.P., Amoozegar, A., Vepraskas, M.J., 1997. Biotite alteration to halloysite and kaolinite in soil-saprolite profiles developed from mica schist and granite gneiss. Geoderma 75, 55–170. https://doi.org/10.1016/S0016-7061(96)00089-4.
Kump, L.R., Brantley, S.L., Arthur, M.A., 2000. Chemical weathering, atmospheric CO2, and climate. Annu. Rev. Earth Planet. Sci. 28, 611–667. https://doi.org/10.1146/annurev.earth.28.1.611.
Laufer, F., Yariv, S., Steiberg, M., 1984. The adsorption of quadrivalent cerium by kaolinite. Clay Miner. 19, 134–149. https://doi.org/10.1180/claymin.1984.019.2.02.
Le Pera, E., Critelli, S., Sorriso-Valvo, M., 2001. Weathering of gneiss in Calabria, Southern Italy. Catena 42, 1–15. https://doi.org/10.1016/S0341-8162(00)00117-X.
Li, L., Maher, K., Navarre-Sitchler, A., Druhan, J., Meile, C., Lawrence, C., Jin, L., 2017. Expanding the role of reactive transport models in critical zone processes. Earth Sci. Rev. 165, 280–301. https://doi.org/10.1016/j.earscirev.2016.09.001.
Li, M.Y.H., Teng, F.Z., Zhou, M.F., 2021. Phyllosilicate controls on magnesium isotopic fractionation during weathering of granites: implications for continental weathering and riverine system. Earth Planet. Sci. Lett. 553, 116613. https://doi.org/10.1016/j.epsl.2020.116613.
Li, Z., Qiu, J.S., Yang, X.M., 2014. A review of the geochronology and geochemistry of Late Yanshanian (Cretaceous) plutons along the Fujian coastal area of southeastern China: Implications for magma evolution related to slab break-off and rollback in the Cretaceous. Earth Sci. Rev. 128, 232–248. https://doi.org/10.1016/j.earscirev.2013.09.007.
Little, M.G., Aeolus Lee, C.-T., 2006. On the formation of an inverted weathering profile on Mount Kilimanjaro, Tanzania: Buried paleosol or groundwater weathering? Chem. Geol. 235, 205–221. https://doi.org/10.1016/j.chemgeo.2006.06.012.
Liu, J., Steinke, S., Vogt, C., Mohtadi, M., De Pol-Holz, R., Hebbeln, D., 2017. Temporal and spatial patterns of sediment deposition in the northern South China Sea over the last 50,000 years. Palaeogeogr. Palaeoclimatol. Palaeoecol. 465, 212–224. https://doi.org/10.1016/j.palaeo.2016.10.033.
Liu, S., Zhang, J., Li, Q., Zhang, L., Wang, W., Yang, P., 2012. Geochemistry and U-Pb zircon ages of metamorphic volcanic rocks of the Paleoproterozoic Lüliang Complex and constraints on the evolution of the Trans-North China Orogen, North China Craton. Precambr. Res. 222–223, 173–190. https://doi.org/10.1016/j.precamres.2011.07.006.
Liu, W., Liu, C., Brantley, S.L., Xu, Z., Zhao, T., Liu, T., Yu, C., Xue, D., Zhao, Z., Cui, L., Zhang, Z., Fan, B., Gu, X., 2016. Deep weathering along a granite ridgeline in a subtropical climate. Chem. Geol. 427, 17–34. https://doi.org/10.1016/j.chemgeo.2016.02.014.
Liu, X.M., Rudnick, R.L., McDonough, W.F., Cummings, M.L., 2013. Influence of chemical weathering on the composition of the continental crust: Insights from Li and Nd isotopes in bauxite profiles developed on Columbia River Basalts. Geochim. Cosmochim. Acta 115, 73–91. https://doi.org/10.1016/j.gca.2013.03.043.
Louvat, P., Alle‘gre, C.J., 1997. Present denudation rates at Re´union island determined by river geochemistry: basalt weathering and mass budget between chemical and mechanical erosions. Geochim. Cosmochim. Acta 61, 3645–3669. https://doi.org/10.1016/s0016-7037(97)00180-4.
Macias, F., Chesworth, W., 1992. Weathering in humid regions, with emphasis on igneous rocks and their metamorphic equivalents. In: Development in Earth Surface Processes 2. Elsevier, Amsterdam, pp. 283–306. https://doi.org/10.1016/B978-0-444-89198-3.50017-9.

Martz, L.W., de Jong, E., 1990. Natural radionuclides in the soils of a small agricultural basin in the Canadian prairies and their association with topography, soil properties and erosion. Catena 17, 85–96. https://doi.org/10.1016/0341-8162(90)90017-8.
Mavris, C., Egli, M., Plötze, M., Blum, J.D., Mirabella, A., Giaccai, D., Haeberli, W., 2010. Initial stages of weathering and soil formation in the Morteratsch proglacial area (Upper Engadine, Switzerland). Geoderma 155 (3–4), 359–371. https://doi.org/10.1016/j.geoderma.2009.12.019.
McLennan, S.M., 1993. Weathering and global denudation. J. Geol. 101 (2), 295–303. https://doi.org/10.2307/30081153.
Mehta, P., 2007. Impact of climate on geochemical mobilization of elements during rock weathering in Kaveri river catchment. Ph. D. Thesis, Jawaharlal Nehru University, New Delhi.
Middelburg, J.J., van der Weijden, C.H., Woittiez, J.R.W., 1988. Chemical processes affecting the mobility of major, minor and trace elements during weathering of granitic rocks. Chem. Geol. 68 (3–4), 253–273. https://doi.org/10.1016/0009-2541(88)90025-3.
Minasny, B., Finke, P., Stockmann, U., Vanwalleghem, T., McBratney, A.B., 2015. Resolving the integral connection between pedogenesis and landscape evolution. Earth Sci. Rev. 150, 102–120. https://doi.org/10.1016/j.earscirev.2015.07.004.
Moore, Reynolds, D.M., Jr, R.C., 1997. X-ray Diffraction and the Identification and Analysis of Clay Minerals. Oxford University Press, New York.
Nascimento, N.R., Bueno, G.T., Fritsch, E., Herbillon, A.J., Allard, T., Melfi, A.J., Astolfo, R., Boucher, H., Li, Y., 2004. Podzolization as a deferralitization process: a study of an Acrisol-Podzol sequence derived from Palaeozoics and stones in the northern upper Amazon basin. Eur. J. Soil Sci. 55, 523–538. https://doi.org/10.1111/j.1365-2389.2004.00616.x.
Ndjigui, P.D., Bilong, P., Bitom, D., Dia, A., 2008. Mobilization and redistribution of major and trace elements in two weathering profiles developed on serpentinites in the Lomié ultramafic complex, South-East Cameroon. J. Afr. Earth Sc. 50, 305–328. https://doi.org/10.1016/j.jafrearsci.2007.10.006.
Nesbitt, H.W., 1979. Mobility and fractionation of rare earth elements during weathering of a granodiorite. Nature 279, 206–210. https://doi.org/10.1038/279206a0.
Nesbitt, H.W., Markovics, G., 1997. Weathering of granodioritic crust, long-term storage of elements in weathering profiles, and petrogenesis of siliciclastic sediments. Geochim. Cosmochim. Acta 61 (8), 1653–1670. https://doi.org/10.1016/s0016-7037(97)00031-8.
Nesbitt, H., Young, G.M., 1982. Early Proterozoic climates and plate motions inferred from major element chemistry of lutites. Nature 299, 715–717. https://doi.org/10.1038/299715a0.
Nesbitt, H.W., Markovics, G., Price, R.C., 1980. Chemical processes affecting alkalis and alkaline earths during continental weathering. Geochim. Cosmochim. Acta 44 (11), 1659–1666. https://doi.org/10.1016/0016-7037(80)90218-5.
Nesbitt, H.W., Young, G.M., 1996. Petrogenesis of sediments in the absence of chemical weathering: effects of abrasion and sorting on bulk composition and mineralogy. Sedimentology 43, 341–358. https://doi.org/10.1046/j.1365-3091.1996.d01-12.x.
Ng, C.W.W., Guan, P., Shang, Y.J., 2001. Weathering mechanisms and indices of the igneous rocks of Hong Kong. Q. J. Eng. Geol. Hydrogeol. 34 (2), 133–151. https://doi.org/10.1144/qjegh.34.2.133.
Oliva, P., Viers, J., Dupré, B., 2003. Chemical weathering in granitic crystalline environments. Chem. Geol. 202, 225–256. https://doi.org/10.1016/j.chemgeo.2002.08.001.
Parker, A., 1970. An index of weathering for silicate rocks. Geol. Mag. 107, 501–504. https://doi.org/10.1017/S0016756800058581.
Phillips, J.D., 2019. Evolutionary pathways in soil-geomorphic systems. Soil Sci. 184 (1), 1–12. https://doi.org/10.1097/SS.0000000000000246.
Phillips, J.D., Turkington, A.V., Marion, D.A., 2008. Weathering and vegetation effects in early stages of soil formation. Catena 72 (1), 21–28. https://doi.org/10.1016/j.catena.2007.03.020.
Pistiner, J.S., Henderson, G.M., 2003. Lithium-isotope fractionation during continental weathering processes. Earth Planet. Sci. Lett. 214 (1–2), 327–339. https://doi.org/10.1016/S0012-821X(03)00348-0.
Podwojewski, P., Poulenard, J., Nguyet, M.L., De Rouw, A., Pham, Q.H., Tran, D.T., 2011. Climate and vegetation determine soil organic matter status in an alpine inner-tropical soil catena in the Fan Si Pan Mountain, Vietnam. Catena 87 (2), 226–239. https://doi.org/10.1016/j.catena.2011.06.002.
Price, J.R., Velbel, M.A., 2003. Chemical weathering indices applied to weathering profiles developed on heterogeneous felsic metamorphic parent rocks. Chem. Geol. 202, 397–416. https://doi.org/10.1016/j.chemgeo.2002.11.001.
Rajamani, V., Tripathi, J.K., Malviya, V.P., 2009. Weathering of lower crustal rocks in the Kaveri river catchment, southern India: implications to sediment geochemistry. Chem. Geol. 265 (3–4), 410–419. https://doi.org/10.1016/j.chemgeo.2009.05.007.
Raymo, M.E., Ruddiman, W.F., 1992. Tectonic forcing of late Cenozoic climate. Nature 359, 117–122. https://doi.org/10.1038/359117a0.
Richter, D.D., Mobley, M.L., 2009. Monitoring Earth's critical zone. Science 326, 1067–1068. https://doi.org/10.1126/science.1179117.
Riebe, C.S., Kirchner, J.W., Finkel, R.C., 2003. Long-term rates of chemical weathering and physical erosion from cosmogenic nuclides and geochemical mass balance. Geochim. Cosmochim. Acta 67, 4411–4427. https://doi.org/10.1016/S0016-7037(03)00382-X.
Riebe, C.S., Kirchner, J.W., Granger, D.E., Finkel, R.C., 2001. Strong tectonic and weak climatic control of long-term chemical weathering rates. Geology 29, 511–514. https://doi.org/10.1130/0091-7613(2001)0292.0.CO;2.
Rihs, S., Gontier, A., Pelt, E., Fries, D., Turpault, M.P., Chabaux, F., 2016. Behavior of U, Th and Ra isotopes in soils during a land cover change. Chem. Geol. 441, 106–123. https://doi.org/10.1016/j.chemgeo.2016.08.016.
Scarciglia, F., Critelli, S., Borrelli, L., Coniglio, S., Muto, F., Perri, F., 2016. Weathering profiles in granitoid rocks of the Sila Massif uplands, Calabria, southern Italy: new insights into their formation processes and rates. Sed. Geol. 336, 46–67. https://doi.org/10.1016/j.sedgeo.2016.01.015.
Scarciglia, F., Le Pera, E., Critelli, S., 2005. Weathering and pedogenesis in the Sila Grande Massif (Calabria, South Italy): from field scale to micromorphology. Catena 61 (1), 1–29. https://doi.org/10.1016/j.catena.2005.02.001.
Sharma, A., Sensarma, S., Kumar, K., Khanna, P.P., Saini, N.K., 2013. Mineralogy and geochemistry of the Mahi River sediments in tectonically active western India: Implications for Deccan large igneous province source, weathering and mobility of elements in a semi-arid climate. Geochim. Cosmochim. Acta 104, 63–83. https://doi.org/10.1016/j.gca.2012.11.004.
Shotyk, W., Weiss, D., Kramers, J.D., Frei, R., Cheburkin, A.K., Gloor, M., Reese, S., 2001. Geochemistry of the peat bog at Etang de la Gruère, Jura Mountains, Switzerland, and its record of atmospheric Pb and lithogenic trace metals (Sc, Ti, Y, Zr, and REE) since 12, 370 14C yr BP. Geochim. Cosmochim. Acta 65, 2337–2360. https://doi.org/10.1016/S0016-7037(01)00586-5.
Souza, J.J.L.L.D., Fontes, M.P.F., Gilkes, R., Costa, L.M.D., Oliveira, T.S.D., 2018. Geochemical signature of Amazon tropical rainforest soils. Revista Brasileira de Ciência do Solo 42. https://doi.org/10.1590/18069657rbcs20170192.
Stallard, R.F., Edmond, J.M., 1983. Geochemistry of the Amazon: 2. The influence of geology and weathering environment on the dissolved load. J. Geophys. Res. Atmos. 88 (C14), 9671–9688. https://doi.org/10.1029/JC088iC14p09671.
Stewart, B.W., Capo, R.C., Chadwick, O.A., 2001. Effects of rainfall on weathering rate, base cation provenance, and Sr isotope composition of Hawaiian soils. Geochim. Cosmochim. Acta 65, 1087–1099. https://doi.org/10.1016/S0016-7037(00)00614-1.
Su, N., Yang, S.Y., Wang, X.D., Bi, L., Yang, C.F., 2015. Magnetic parameters indicate the intensity of chemical weathering developed on igneous rocks in China. Catena 133, 328–341. https://doi.org/10.1016/j.catena.2015.06.003.
Su, N., Yang, S., Guo, Y., Yue, W., Wang, X., Yin, P., Huang, X., 2017. Revisit of rare earth element fractionation during chemical weathering and river sediment transport. Geochem. Geophys. Geosyst. 18 (3), 935–955. https://doi.org/10.1002/2016GC006659.
Taboada, T., García, C., 1999. Smectite formation produced by weathering in a coarse granite saprolite in Galicia (NW Spain). Catena 35, 281–290. https://doi.org/10.1016/S0341-8162(98)00107-6.
Tadini, A.M., Nicolodelli, G., Senesi, G.S., Ishida, D.A., Montes, C.R., Lucas, Y., Mounier, S., Guimarães, F.E.G., Milori, D.M.B.P., 2018. Soil organic matter in podzol horizons of the Amazon region: humification, recalcitrance, and dating. Sci. Total Environ. 613, 160–167. https://doi.org/10.1016/j.scitotenv.2017.09.068.
Tardy, Y., 1997. Petrology of Laterites and Tropical Soils. Balkema, Rotterdam, p. 408.
Tardy, Y., Bocquier, G., Paquet, H., Millot, G., 1973. Formation of clay from granite and its distribution in relation to climate and topography. Geoderma 10, 271–284. https://doi.org/10.1016/0016-7061(73)90002-5.
Taylor, S.R., McLennan, S.M., 1985. The continental crust: its composition and evolution. Blackwell Scientific Publications, Oxford.
Thorpe, M.T., Hurowitz, J.A., 2020. Unraveling sedimentary processes in fluvial sediments from two basalt dominated watersheds in northern Idaho, USA. Chem. Geol. 550, 119673. https://doi.org/10.1016/j.chemgeo.2020.119673.
Thorpe, M.T., Hurowitz, J.A., Dehouck, E., 2019. Sediment geochemistry and mineralogy from a glacial terrain river system in southwest Iceland. Geochim. Cosmochim. Acta 263, 140–166. https://doi.org/10.1016/j.gca.2019.08.003.
Kamp, P.C.V.D., 2010. Arkose, subarkose, quartz sand, and associated muds derived from felsic plutonic rocks in glacial to tropical humid climates. J. Sediment. Res. 80 (10), 895–918. https://doi.org/10.2110/jsr.2010.081.
Vitousek, P.M., Porder, S., Houlton, B.Z., Chadwick, O.A., 2010. Terrestrial phosphorus limitation: mechanisms, implications, and nitrogen–phosphorus interactions. Ecol. Appl. 20 (1), 5–15. https://doi.org/10.1890/08-0127.1.
von Blanckenburg, F., Hewawasam, T., Kubik, P.W., 2004. Cosmogenic nuclide evidence for low weathering and denudation in the wet, tropical highlands of Sri Lanka. J. Geophys. Res. 109, F03008. https://doi.org/10.1029/2003JF000049.
Walker, J.C., Hays, P.B., Kasting, J.F., 1981. A negative feedback mechanism for the long-term stabilization of Earth's surface temperature. J. Geophys. Res. Oceans 86 (C10), 9776–9782. https://doi.org/10.1029/JC086iC10p09776.
Wallmann, K., Aloisi, G., Haeckel, M., Tishchenko, P., Pavlova, G., Greinert, J., Eisenhauer, A., 2008. Silicate weathering in anoxic marine sediments. Geochim. Cosmochim. Acta 72 (12), 2895–2918. https://doi.org/10.1016/j.gca.2008.03.026.
Wan, S., Li, A., Clift, P.D., Wu, S., Xu, K., Li, T., 2010. Increased contribution of terrigenous supply from Taiwan to the northern South China Sea since 3 Ma. Mar. Geol. 278 (1–4), 115–121. https://doi.org/10.1016/j.margeo.2010.09.008.
Wan, S.M., Li, A.C., Clift, P.D., Stutt, J.B., 2007. Development of the East Asian monsoon: mineralogical and sedimentologic records in the northern South China Sea since 20 Ma. Palaeogeogr. Palaeoclimatol. Palaeoecol. 254, 561–582. https://doi.org/10.1016/j.palaeo.2007.07.009.
Weber, K.A., Achenbach, L.A., Coates, J.D., 2006. Microorganisms pumping iron: anaerobic microbial iron oxidation and reduction. Nat. Rev. Microbiol. 4, 752–764. https://doi.org/10.1038/nrmicro1490.
Wei, G., Li, X.H., Liu, Y., Shao, L., Liang, X., 2006. Geochemical record of chemical weathering and monsoon climate change since the early Miocene in the South China Sea. Paleoceanography 21 (4). https://doi.org/10.1029/2006PA001300.
West, A.J., Galy, A., Bickle, M., 2005. Tectonic and climatic controls on silicate weathering. Earth Planet. Sci. Lett. 235, 211–228. https://doi.org/10.1016/j.epsl.2005.03.020.

White, A.F., Blum, A.E., 1995. Effects of climate on chemical weathering in watersheds. Geochim. Cosmochim. Acta 59, 1729–1747. https://doi.org/10.1180/minmag.1994.58A.2.238.

Wilson, M.J., 1999. The origin and formation of clay minerals in soils: past, present and future perspectives. Clay Miner. 34, 7–25. https://doi.org/10.1180/000985599545957.

Wimpenny, J., Yin, Q.Z., Tollstrup, D., Xie, L.W., Sun, J., 2014. Using Mg isotope ratios to trace Cenozoic weathering changes: a case study from the Chinese Loess Plateau. Chem. Geol. 376, 31–43. https://doi.org/10.1016/j.chemgeo.2014.03.008.

Yaalon, D.H., 1997. Soils in the Mediterranean region: what makes them different? Catena 28 (3–4), 157–169. https://doi.org/10.1016/S0341-8162(96)00035-5.

Young, G.M., Nesbitt, H.W., 1998. Processes controlling the distribution of Ti and Al in weathering profiles, siliciclastic sediments and sedimentary rocks. J. Sediment. Res. 68 (3), 448–455. https://doi.org/10.2110/jsr.68.448.

Zhu, Y., Duan, G., Chen, B., Peng, X., Chen, Z., Sun, G., 2014. Mineral weathering and element cycling in soil-microorganism-plant system. Sci. China Earth Sci. 57 (5), 888–896. https://doi.org/10.1007/s11430-014-4861-0.